

# Bjerknæs Compensation in Meridional Heat Transport under Freshwater Forcing and the Role of Climate Feedback

HAIJUN YANG, QIN WEN, AND JIE YAO

*Laboratory for Climate and Ocean–Atmosphere Studies, and Department of Atmospheric and Oceanic Sciences, School of Physics, Peking University, Beijing, China*

YUXING WANG

*National Marine Environmental Forecasting Center, State Oceanology Administration, Beijing, China*

(Manuscript received 18 November 2016, in final form 10 March 2017)


## ABSTRACT

Using a coupled Earth climate model, freshwater forcing experiments are performed to study the Bjerknæs compensation (BJC) between meridional atmosphere heat transport (AHT) and meridional ocean heat transport (OHT). Freshwater hosing in the North Atlantic weakens the Atlantic meridional overturning circulation (AMOC) and thus reduces the northward OHT in the Atlantic significantly, leading to a cooling (warming) in the surface layer in the Northern (Southern) Hemisphere. This results in an enhanced Hadley cell and northward AHT. Meanwhile, the OHT in the Indo-Pacific is increased in response to the Hadley cell change, partially offsetting the reduced OHT in the Atlantic. Two compensations occur here: compensation between the AHT and the Atlantic OHT, and that between the Indo-Pacific OHT and the Atlantic OHT. The AHT change undercompensates the OHT change by about 60% in the extratropics, while the former overcompensates the latter by about 30% in the tropics due to the Indo-Pacific change. The BJC can be understood from the viewpoint of large-scale circulation change. However, the intrinsic mechanism of BJC is related to the climate feedback of the Earth system. The authors' coupled model experiments confirm that the occurrence of BJC is an intrinsic requirement of local energy balance, and local climate feedback determines the extent of BJC, consistent with previous theoretical results. Even during the transient period of climate change, the BJC is well established when the ocean heat storage is slowly varying and its change is much weaker than the net local heat flux change at the ocean surface. The BJC can be deduced from the local climate feedback. Under the freshwater forcing, the overcompensation in the tropics is mainly caused by the positive longwave feedback related to clouds, and the undercompensation in the extratropics is due to the negative longwave feedback related to surface temperature change. Different dominant feedbacks determine different BJC scenarios in different regions, which are in essence constrained by local energy balance.

## 1. Introduction

Meridional heat transports (MHTs) in the atmosphere and ocean are critical for maintaining energy balance of Earth's climate system. The combined atmosphere and ocean heat transports have a peak value of about 5.5 PW (1 PW =  $10^{15}$  W) at 35°N/S (Trenberth and Caron 2001). The ocean heat transport (OHT) dominates in the deep tropics while the atmosphere heat

transport (AHT) dominates poleward of 30°N/S (Held 2001; Wunsch 2005; Czaja and Marshall 2006). This mean structure is well recognized. However, the MHT change receives the most attention. There is a so-called Bjerknæs compensation (BJC) in the Earth heat transport, stating that changes in OHT and AHT should perfectly compensate each other (Bjerknæs 1964) if one neglects changes in the net radiation forcing at the top of the atmosphere (TOA) and the ocean heat storage as well as possible energetic inconsistencies introduced in models.

 Denotes content that is immediately available upon publication as open access.

Corresponding author: Haijun Yang, hjyang@pku.edu.cn



This article is licensed under a Creative Commons Attribution 4.0 license (<http://creativecommons.org/licenses/by/4.0/>).

The BJC is important since it may play a critical role in maintaining the overall stability of the Earth climate system. It has been studied extensively in recent years, using a large variety of models (e.g., North 1984; Langen and Alexeev 2007; Rose and Ferreira 2013; Liu et al. 2016; Shaffrey and Sutton 2006; Cheng et al. 2007; van der Swaluw et al. 2007; Kang et al. 2008, 2009; Vellinga and Wu 2008; Yang et al. 2013; Seo et al. 2014; Yang and Dai 2015). The BJC can occur in internal climate variability (e.g., Shaffrey and Sutton 2006) and in climate responses to external forcing (e.g., Vellinga and Wu 2008; Rose and Ferreira 2013; Yang and Dai 2015). However, the compensation structure and mechanisms in these studies can be different. The BJC can be perfect either in high latitudes (Shaffrey and Sutton 2006; Cheng et al. 2007) or near the equator (Vellinga and Wu 2008). In the latter scenario, the compensation structure can be different among different models. In Vellinga and Wu (2008), the compensation is very efficient at low latitudes and nearly complete at the equator. The maximum AHT change occurs right on the equator while the maximum OHT change occurs near 20°N. In Zhang and Delworth (2005) the maximum AHT change occurs around 15°–20°N. In Cheng et al. (2007), the compensation is good from the low latitudes to 40°N. The maximum changes in AHT and OHT occur around 20°–30°N. The BJC behaviors are substantially different in different studies. Large controversies remain with regard to the fundamental mechanism of BJC.

Recent theoretical studies of Liu et al. (2016) and Yang et al. (2016b) have revealed that the local climate feedback between the net TOA heat flux and surface temperature determines the BJC. The BJC rate is defined as the ratio of anomalous AHT ( $\Delta F_a$ ) to anomalous OHT ( $\Delta F_o$ ) [ $C_R \equiv (\Delta F_a/\Delta F_o)$ ], which is found to depend only on the local climate feedback ( $B$ ) [ $C_R \sim -(1/1 - B)$ ]. The overcompensation ( $|C_R| > 1$ ), perfect compensation ( $|C_R| = 1$ ), or undercompensation ( $|C_R| < 1$ ) of the AHT to the OHT is due to a positive feedback ( $B > 0$ ), zero feedback ( $B = 0$ ), or negative feedback ( $B < 0$ ), respectively. The different BJC behaviors in various modeling studies can be attributed to different climate feedbacks. The theoretical studies revealed the fundamental mechanism of BJC and provided a unified explanation on the BJC behaviors in different studies. Liu et al. (2016) and Yang et al. (2016b) further concluded that it is the global energy conservation that determines whether the BJC occurs or not, while how the BJC occurs is determined by the local climate feedback.

This work is a part of our series of studies on BJC in the Earth climate system (Yang and Dai 2015; Dai et al. 2017; Yang et al. 2016b; Zhao et al. 2016). Using a coupled Earth system model, we have investigated the

intrinsic mechanism of BJC through a set of wind-perturbation experiments (Dai et al. 2017) and concluded that the energy constraint indeed determines the occurrence of the BJC, and the local climate feedback determines how the BJC occurs, regardless of different climate responses in different wind perturbation situations. This is consistent with the theoretical studies of Liu et al. (2016) and Yang et al. (2016b). In this work, we further investigate the BJC and the roles of energy conservation and climate feedback through freshwater perturbation experiments. Freshwater hosing in the North Atlantic weakens the Atlantic meridional overturning circulation (AMOC) and thus reduces the northward OHT in the Atlantic significantly, leading to a cooling (warming) in surface layer in the Northern (Southern) Hemisphere. These changes are robust and consistent among different climate models (e.g., Zhang and Delworth 2005; Shaffrey and Sutton 2006; Cheng et al. 2007; Vellinga and Wu 2008). Two compensations are found here: compensation between the AHT and the Atlantic OHT, and compensation between the Indo-Pacific OHT and Atlantic OHT. The AHT change compensates the OHT change very well (about 60%) in the extratropics, while the former overcompensates the latter by about 30% in the tropics due to the Indo-Pacific change. Freshwater experiments also confirm that the occurrence of BJC is an intrinsic requirement of local energy balance, and local climate feedback determines the extent of BJC. We further disclose that even during the transient period of climate change, the BJC can be well established if the ocean heat storage is slowly varying and its change is much weaker than the net local heat flux change at the ocean surface. The BJC rate can be deduced from local climate feedback. Different from previous studies, we emphasize that the BJC at a given latitude is determined by the climate feedbacks of nearby regions, rather than by the heat budget at the latitude.

This paper is organized as follows. An introduction to the model and experiments is given in section 2. Transient and equilibrium responses to the freshwater perturbation in a coupled model are analyzed in section 3. The BJC, energy balance, and climate feedbacks in regional boxes are examined in detail in section 4. A summary and discussion are given in section 5. Detailed information about the radiation flux at the TOA, clouds, and cloud radiation forcing are presented in the appendix.

## 2. Model and experiments

The model used in this study is same as that used in Dai et al. (2017), that is, the Community Earth System Model (CESM) version 1.0 of the National Center for Atmospheric Research (NCAR). Here we simply repeat

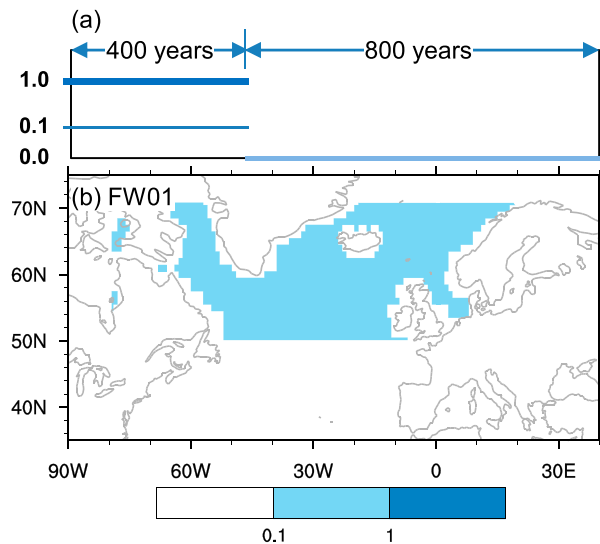


FIG. 1. Schematic plot showing the freshwater forcing used in FW01: (a) the freshwater hosing persists for 400 yr and is then stopped for the 800-yr integration thereafter, and (b) 0.1-Sv freshwater is uniformly injected into the North Atlantic basin ( $50^{\circ}$ – $70^{\circ}$ N).

the model description as in Dai et al. (2017). CESM is a fully coupled global climate model that provides state-of-the-art simulations of the Earth's past, present, and future climate states (<http://www.cesm.ucar.edu/>). CESM1.0 consists of five components and one coupler: the Community Atmosphere Model (CAM5; Park et al. 2014), the Community Land Model (CLM4; Lawrence et al. 2012), the Los Alamos Sea Ice Model (CICE4; Hunke and Lipscomb 2010), the Parallel Ocean Program (POP2; Smith et al. 2010), the Community Ice Sheet Model (Glimmer-CISM), and the CESM Coupler (CPL7). CESM1.0 has been widely used and validated by researchers in the community (<http://journals.ametsoc.org/page/CCSM4/CESM1>).

The model grid employed in this study is T31\_gx3v7. The CAM5 has 26 vertical levels, with the finite volume nominally  $3.75^{\circ} \times 3.75^{\circ}$  in the horizontal. It is essentially a new atmospheric model with more realistic formulations of radiation, boundary layer, and aerosols (Meehl et al. 2013; Neale et al. 2013). The general features of the model formulation were given by Neale et al. (2010) and Park et al. (2014). The CLM4 has the same horizontal resolution as the CAM5. The POP2 uses the grid gx3v7, which has 60 vertical levels and a uniform  $3.6^{\circ}$  spacing in the zonal direction. In the meridional direction, the grid is nonuniformly spaced: it is  $0.6^{\circ}$  near the equator, gradually increasing to the maximum  $3.4^{\circ}$  at  $35^{\circ}$ N/S and then decreasing poleward. The model physics is described in details in Danabasoglu et al. (2012). The CICE4 has the same horizontal grid as the POP2. No flux adjustments are used in CESM1.0.

Experiments analyzed in this study include a 2700-yr control run (CTRL) and two 1200-yr freshwater perturbation runs. The CTRL starts from the rest with standard configurations (<http://www.cesm.ucar.edu/experiments/cesm1.0/>). The model climate as a whole reaches quasi-equilibrium after 1000 years of integration (Yang et al. 2015a). The freshwater perturbation experiments start from year 1500 of CTRL, in which 0.1-Sv (experiment FW01) and 1.0-Sv (experiment FW10) freshwater amounts ( $1 \text{ Sv} = 10^6 \text{ m}^3 \text{ s}^{-1}$ ) are hosed uniformly into the North Atlantic basin ( $50^{\circ}$ – $70^{\circ}$ N,  $70^{\circ}$ W– $15^{\circ}$ E) for 400 years (Fig. 1), respectively. This freshwater is converted to freshwater flux and included in the surface level of salinity equation of the ocean model. After the 400-yr integration, the freshwater hosing is ceased suddenly, and the experiments continue to integrate for 800 years. During the water hosing stage, FW01 and FW10 reach quasi-equilibrium after 400-yr integration. During the ceased water hosing stage, the two experiments reach quasi-equilibrium after 600-yr integration. Two equilibrium stages are defined for later analysis (Fig. 2): stage I is from year 200 to year 400, representing the equilibrium stage for the freshwater forcing, during which the AMOC remains in a nearly shut-down state (Fig. 5); stage II is from year 1000 to year 1200, representing the equilibrium stage after the AMOC recovers to the normal level of CTRL (Fig. 5). The equilibrium responses in stage I are obtained by subtracting mean states in the CTRL. The equilibrium responses in stage II are obtained by subtracting the mean states in stage I. Since the climate responses in FW10 are very similar to those in FW01, in the following sections only the results from FW01 are discussed in details. In general, the AMOC is reduced by 80% in stage I in response to the freshwater hosing in the North Atlantic basin, and it then takes about 500 years to recover to the normal state after ceasing the freshwater hosing (Fig. 5).

### 3. Transient and equilibrium responses

#### a. Energy balance at the TOA

The net radiation flux at the TOA reaches quasi-equilibrium during stages I and II (Fig. 2a). The changes in the net downward shortwave radiation (SW) and the net outgoing longwave radiation (LW) at the TOA are in phase at most latitudes. In other words, a decrease (increase) in the downward SW can be roughly compensated by a decrease (increase) in the upward LW, leaving a trivial change in the net radiation flux at the TOA. The equilibrium changes in SW and LW at the TOA in FW01 are less than 5% of their corresponding total values (5 PW) (Fig. 2b). At most latitudes, the in-phase changes between SW and LW are nearly perfect (Fig. 2b), leaving the net radiation flux roughly

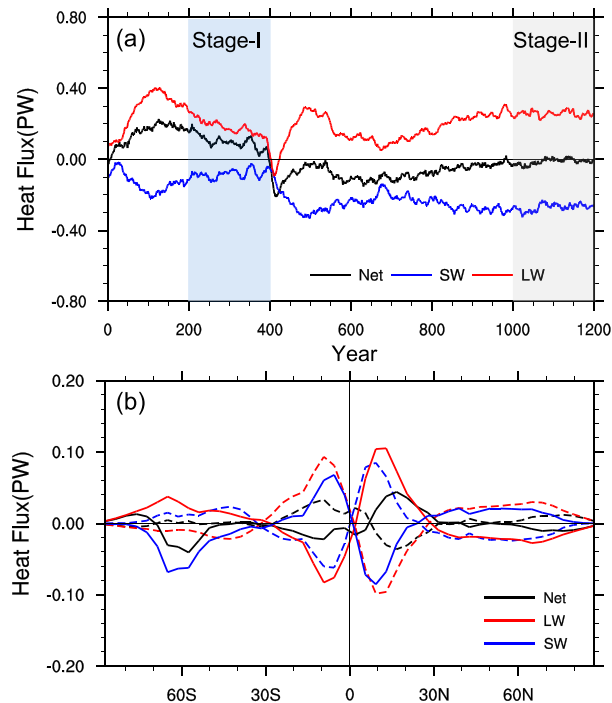


FIG. 2. (a) Temporal change of the globally integrated net radiation flux (black), net downward shortwave (SW, blue), and net outgoing longwave (LW, red) at the top of atmosphere (TOA) in FW01. The mean values from the control experiment (CTRL) are subtracted. The curves are smoothed with an 11-yr running mean. Stage I spans over years 200–400, representing the equilibrium stage in response to freshwater hosing. Stage II spans over years 1000–1200, representing an equilibrium stage after the freshwater hosing is ceased. (b) The equilibrium changes of the TOA radiation flux in stage I (dashed curves) and stage II (solid curves) of FW01. In stage I, the mean values from the CTRL are subtracted. In stage II, the mean values from stage I are removed. The radiation flux has been converted to radiation heat transport by multiplying the surface area of each latitude band, for better comparison with other figures. Positive values represent net downward flux change, namely, a positive LW (SW) change represents a decrease (increase) in the outgoing LW (downward SW). Units: PW ( $1 \text{ PW} = 10^{15} \text{ W}$ ).

unchanged, particularly in stage II. The reasons for the SW and LW changes in different latitudes and stages in FW01 are discussed in detail in the [appendix](#). In general, the compensation change between SW and LW leads to a small change in the net radiation flux at the TOA, even during the transient stage of freshwater forcing ([Fig. 2a](#)), suggesting that Earth's climate as a whole tends to be steady under freshwater perturbation and the global energy conservation is well satisfied.

### b. Changes in global oceans

The equilibrium responses in sea surface salinity (SSS), temperature (SST), and density (SSD) of FW01 are shown in [Fig. 3](#). In stage I, it is straightforward that the North

Atlantic surface freshening ([Fig. 3a](#)) is mainly due to the freshwater hosing at the high latitudes. The cessation of the salinity advection from the tropics also contributes to the surface freshening at the midlatitudes ([Timmermann and Goosse 2004](#); [Yang et al. 2016a](#)). The shutdown of the AMOC results in a significant weakening (about 40%) of northward heat transport, causing a significant dipole change in the upper-ocean temperature in the Atlantic, with strong surface cooling in the north and weak warming in the south ([Fig. 3b](#)). A similar SST response occurs in the Pacific and Indian Oceans through atmospheric teleconnection. It is also seen that the SSS change dominates the SSD change ([Fig. 3c](#)), and thus the AMOC change. In fact, these changes in response to the freshwater hosing in the North Atlantic have been well recognized in many studies (e.g., [Manabe and Stouffer 1995](#); [Zhang and Delworth 2005](#); [Stouffer et al. 2006, 2007](#); [Cheng et al. 2007](#); [Wu et al. 2007](#); [Chang et al. 2008](#); [Vellinga and Wu 2008](#); [Laurian et al. 2009](#); [Yang et al. 2013](#)).

In stage II, the changes in SSS, SST, and SSD ([Figs. 3d–f](#)) are nearly perfectly opposite to those in stage I, suggesting that Earth's climate could be recovered under the freshwater perturbation. The residual changes, defined as the difference between stage II of FW01 and CTRL, are very small ([Figs. 3g–i](#)). The 0.1-Sv freshwater hosed for 400 years is uniformly distributed and causes about 1-psu salinity reduction over the global ocean ([Fig. 3g](#)). The surface ocean is also uniformly cooled by about  $1^\circ\text{C}$ , except that in the Southern Ocean where a stronger cooling occurs ([Fig. 3h](#)). This cooling is due to sea ice positive feedback in the Southern Hemisphere (SH) ([Fig. 3e](#)). The ultimate SSD is barely affected ([Fig. 3i](#)). The position of the intertropical convergence zone (ITCZ) is illustrated in [Figs. 3b and 3e](#). The ITCZ shift in FW01 is not obvious, which may be due to the coarse resolution of the atmosphere model (about  $3.75^\circ$ ). Detailed reports of residual changes in other climate variables will be presented in other papers, as we want to focus on the understanding of MHT changes in FW01 and the mechanisms for the energy compensation.

The global ocean temperature has a weak drift in response to freshwater hosing. Although the SST has a cooling shift ([Fig. 3h](#)), the total global ocean temperature rises by about  $0.3^\circ\text{C}$  in stage I of FW01 and maintains about a  $0.1^\circ\text{C}$  warming in stage II ([Fig. 4a](#)). In stage I, the ocean warming is manifested in the subsurface near 200–2000 m ([Fig. 4b](#)) and is particularly clear in the Atlantic ([Fig. 4c](#)). The maximum subsurface warming can be above  $1^\circ\text{C}$  at 1000-m depth in the middle-to-high latitudes of the North Atlantic. The subsurface warming in the Pacific is much smaller than that in the Atlantic ([Fig. 4d](#)). After we stop applying the freshwater hosing,



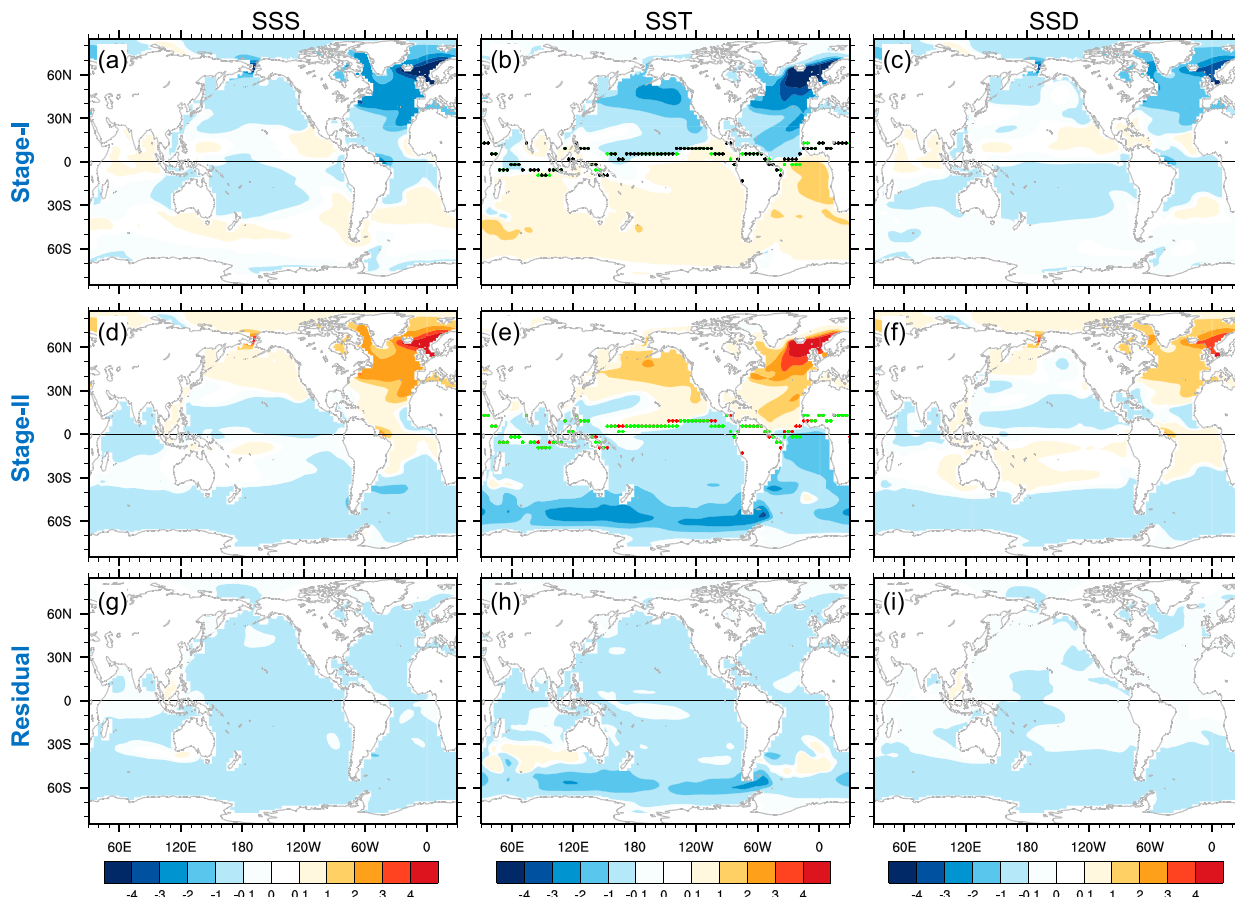


FIG. 3. Equilibrium responses in (a),(d) sea surface salinity (SSS; psu), (b),(e) sea surface temperature (SST; °C), and (c),(f) sea surface density (SSD;  $\text{kg m}^{-3}$ ) in (top) stage I and (middle) stage II of FW01. (g)–(i) The sum of the upper panels, representing the overall effect of 400-yr freshwater hosing on the global ocean. As defined in Fig. 2, stage I spans over years 200–400, representing the equilibrium stage in response to freshwater hosing, and the mean values from the CTRL are subtracted. Stage II spans over years 1000–1200, representing an equilibrium stage after the freshwater hosing is ceased, and the mean values from stage I are removed. The green, black, and red dots represent the ITCZ location in CTRL and stages I and II of FW01, respectively, which is defined as the location of the maximum convergence of surface winds near the equator.

the ocean temperature changes in the opposite direction (Fig. 4a) and finally the subsurface warming is almost damped in stage II, leaving only some warming in the Southern Ocean (Figs. 4e–g). The subsurface warming in stage I (cooling in stage II), which is opposite to the SST change in the Northern Hemisphere (NH), is the result of a baroclinic response of ocean thermal structure to the surface freshwater forcing and has been investigated comprehensively in previous studies (e.g., Manabe and Stouffer 1995; Zhang and Delworth 2005; Stouffer et al. 2007; Chang et al. 2008). The important information we get here is that the ocean heat storage is evolving slowly even after the ocean circulation reaches equilibrium (Fig. 5a). The ocean heat storage increase in stage I nearly disappears in stage II, but a significant warm temperature anomaly still remains below the surface in the Southern Ocean (Fig. 4e). The ocean heat

storage change matters here because it affects the meridional OHT and thus the BJC. We will explore the validity of the BJC in stage II in the next section.

### c. Overturning circulations

The global atmospheric and oceanic overturning circulations change significantly during the freshwater hosing stage and then recover to the mean state of the CTRL after the freshwater hosing stops (Fig. 5a). In stage I, the AMOC is weakened by nearly 80%. The northern branches of the Indo-Pacific subtropical cell (STC) and the atmospheric Hadley cell (HC) are enhanced by about 20%, while their southern branches are weakened by 15%. In stage II, the global atmospheric and oceanic overturning circulations recover toward the CTRL. The STC and HC reach quasi-equilibrium in 200 years. The AMOC overshoots its quasi-equilibrium

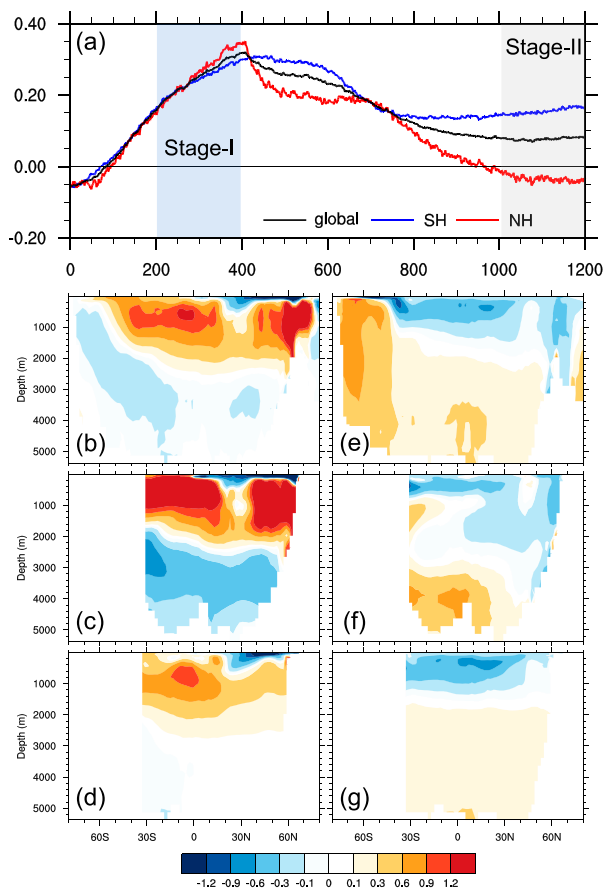


FIG. 4. (a) Temporal evolution of global ocean temperature ( $^{\circ}\text{C}$ ) in FW01. Black, blue, and red curves are for the ocean temperature changes averaged globally and for the Southern Hemisphere (SH) and Northern Hemisphere (NH), respectively. (b)–(d) The zonal-mean temperature responses ( $^{\circ}\text{C}$ ) in stage I of FW01 for the global ocean, the Atlantic, and the Pacific, respectively. (e)–(g) As in (b)–(d), but for stage II of FW01.

state by about 20% during its recovery period and settles after about 400 years.

The evolutions of overturning circulations show in-phase changes between the HC and STC, and out-of-phase (in phase) changes between the AMOC and HC in the NH (in the SH) (Fig. 5a). Note that the curves in Fig. 5a are normalized by their mean values in CTRL, so that the relative changes are clearly demonstrated. These relative changes in the atmosphere and ocean circulations can be understood as follows. During stage I of FW01, the weakening of AMOC (Fig. 5c) leads to surface cooling (warming) in the NH (SH) (Fig. 3b), which consequently forces a southward shift of the ascending branch of tropical atmosphere circulation. Under this background change, the HC in the boreal winter is enhanced due to the enhanced ascending atmosphere circulation in the SH tropics. The HC in the boreal

summer is weakened because the enhanced ascending in the SH tropics counteracts the atmospheric descending at the same latitudes. Therefore, the annual-mean HC is strengthened in the NH and weakened in the SH (Fig. 5b), showing out-of-phase (in phase) change with that of AMOC in the NH (SH). The wind-driven Indo-Pacific STC changes accordingly in response to the HC change (Fig. 5d). The northern (southern) branch of STC is strengthened (weakened), showing a strong coupling with the HC (Liu 1994; Zhang et al. 2010; Held 2001). During the stage of ceased freshwater hosing, the abovementioned processes are reversed.

#### d. Meridional heat transport

The structure of climatological MHT is well known and shown in (Fig. 6a). In the freshwater experiments, significant changes occur in both AHT and OHT (Fig. 6b). The peak change in AHT occurs at the equator, while that in OHT occurs at the NH midlatitudes during stages I and II (Fig. 6b). The latter is attributed to the OHT change in the Atlantic (Fig. 6d). The compensation changes in OHT and AHT occur at almost all latitudes and in both stages of FW01 (Fig. 6b). In the tropics ( $30^{\circ}\text{S}$ – $30^{\circ}\text{N}$ ), the AHT change overcompensates the OHT change, while in the extratropics the AHT change undercompensates the OHT change (Fig. 6b). The main reason is that in the tropics the OHT change in the Indo-Pacific partially offsets the OHT change in the Atlantic (Fig. 6d). In stage I, the HC change (Fig. 5b) results in a northward anomalous AHT in both hemispheres throughout the year (Fig. 6b). The wind-driven Indo-Pacific STC changes in phase with the HC (Fig. 5d) (Held 2001), as does the OHT in the Indo-Pacific (Fig. 6d). The weakened northward OHT in the Atlantic is compensated by both AHT and the enhanced northward OHT in the Indo-Pacific. This compensation structure (Figs. 6b,d) suggests that the AMOC plays a critical role in the global energy balance. The AHT and OHT changes in stage II are nearly symmetric to the changes in stage I, suggesting that Earth's overall energy balance can be recovered under the freshwater perturbation. Here, we want to emphasize that the OHT and AHT in Fig. 6 are calculated directly from the VT approach (using velocity–potential temperature fields; Yang et al. 2015a), instead of indirectly using the heat flux budgets at the ocean surface and the TOA. This assures the independence of AHT and OHT. The ocean heat storage change (Fig. 4) appears to be weak and does not cause the failure of BJC.

In summary, under freshwater perturbation there are two compensations in the MHT: compensation between the Atlantic and Indo-Pacific, and that between the Atlantic and the atmosphere. The Indo-Pacific OHT change

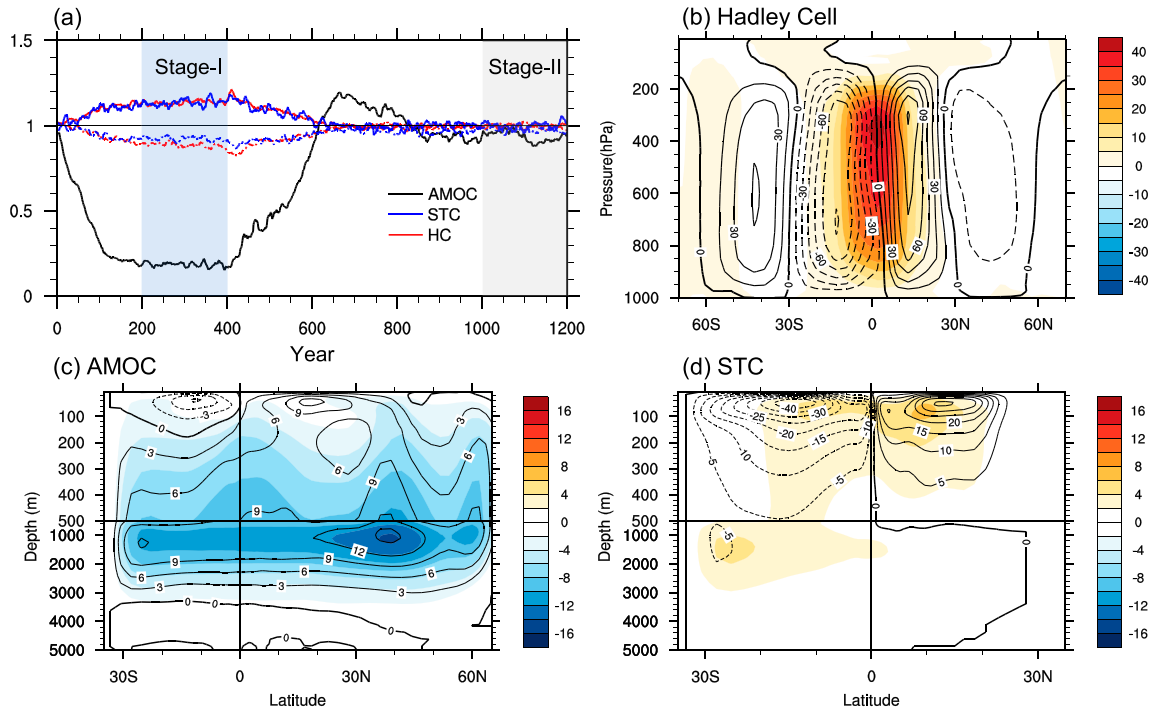


FIG. 5. (a) Temporal evolutions of the Atlantic meridional overturning circulation (AMOC, black), the Indo-Pacific subtropical cell (STC, blue), and the Hadley cell (HC, red) in FW01. (b)–(d) Annual-mean patterns of HC, AMOC, and STC in the CTRL (contours) and their changes in stage I of FW01 (shading), respectively. In (a), the AMOC index is defined as the maximum value of the streamfunction in the range of  $0^{\circ}$ – $10^{\circ}$ C isothermal level over  $20^{\circ}$ – $70^{\circ}$ N in the Atlantic. The Indo-Pacific STC is similarly defined, but in the range of  $20^{\circ}$ – $30^{\circ}$ C over  $0^{\circ}$ – $30^{\circ}$ N for the north branch of STC (solid blue) and over  $30^{\circ}$ S– $0^{\circ}$  for the south branch (dashed blue). The HC index is defined as the maximum value between 200–1000 hPa over  $0^{\circ}$ – $30^{\circ}$ N (north branch; solid red) and  $30^{\circ}$ S– $0^{\circ}$  (south branch; dashed red). All indexes are normalized by their time-mean values in the CTRL, which are 21, 39, and 93 Sv for the AMOC, STC and HC, respectively. Here,  $1 \text{ Sv} = 10^6 \text{ m}^3 \text{ s}^{-1}$  for the ocean and  $1 \text{ Sv} = 10^9 \text{ kg s}^{-1}$  for the atmosphere. In (a), all curves are smoothed with an 11-yr running mean.

can compensate the Atlantic OHT change by about 30%–50% in the tropics (Fig. 6d). The overcompensation of the AHT to the global OHT results from the readjustment of the wind-driven circulation in the Indo-Pacific. In fact, the compensation between the AHT and Atlantic OHT is excellent in the tropics, as shown by the red curves in Fig. 6b and the blue curves in Fig. 6d.

As we have done in Dai et al. (2017), the overall compensation between AHT and OHT can be quantified as the BJC rate  $C_R = r(\sigma_{F_a}/\sigma_{F_o})$  (Zhao et al. 2016), where  $r$  is the correlation coefficient between AHT and OHT over all latitudes;  $\sigma_{F_a}$  and  $\sigma_{F_o}$  are standard deviations of AHT and OHT, respectively, with respect to the latitudes. Having only negative correlation ( $r < 0$ ) suggests a compensation, and the degree of BJC is determined by both the correlation and the ratio of the standard deviations of AHT and OHT. If correlation is low ( $r \rightarrow 0$ ), there will be no meaningful compensation. Naturally, positive correlation ( $r \geq 0$ ) suggests no compensation.

In general, the AHT change compensates the OHT change nearly perfectly in the freshwater experiments if

all latitudes are considered. The BJC is quantified in Table 1. The global overall BJC rate is  $-0.97$  in stage I and  $-1.11$  in stage II. However, in the tropics the AHT overcompensates the OHT by about 20% in stage I and by 50% in stage II. In the extratropics, the AHT undercompensates the OHT by about 40% in both stages I and II. In fact, the overcompensation in the tropics is due to the Indo-Pacific OHT change as mentioned before, which can offset the Atlantic OHT change by about 30%–50% (Table 1). The AHT change can actually compensate the Atlantic OHT change by about 90%.

Under freshwater perturbation, the BJC occurs not only in the equilibrium stage but also during the transient stage (Fig. 7). The compensation situations are different at different latitudes. Figure 7 shows the transient changes in AHT and OHT and their partitions in the Atlantic and Indo-Pacific. In the extratropical NH ( $30^{\circ}$ – $70^{\circ}$ N), the AHT undercompensates the OHT because the Atlantic determines the global total OHT (Fig. 7a). The extratropical OHT change in the Indo-Pacific is negligible. The extratropical AHT change, mainly due to the change in eddy activities

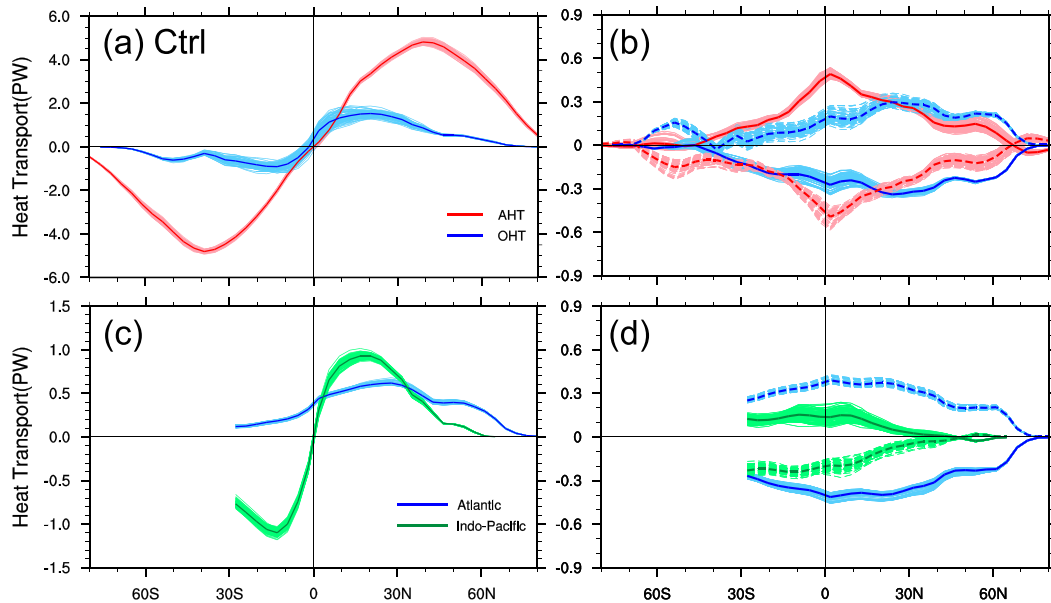


FIG. 6. (a) AHT (red) and global total OHT (blue) in CTRL, and (b) their changes in FW01. Units: PW. The global total OHT in (a) and its change in (b) can be further partitioned into (c) OHT in the Atlantic (blue) and Indo-Pacific (green) and (d) their changes. In (b) and (d), solid curves are for stage I and dashed curves, for stage II. In all plots, thick curves represent 200-yr-mean values; light color curves are for individual years, but smoothed with an 11-yr running mean. The light colors show qualitatively the spread of each variable at decadal and longer time scales. The overall BJC rates are  $-0.97$  and  $-1.11$  in stages I and II of FW01, respectively. The Indo-Pacific OHT change compensates the Atlantic OHT by 30% and 50% in stages I and II, respectively.

(figure not shown), is not strong enough to offset the OHT change. In the tropics ( $30^{\circ}\text{S}$ – $30^{\circ}\text{N}$ ), both changes in AHT and wind-driven OHT are strong and they jointly produce a good compensation between the AHT and OHT (Fig. 7b). In the extratropical SH ( $30^{\circ}$ – $70^{\circ}\text{S}$ ), the AHT compensates the OHT very well during the freshwater hosing stage, but significantly overcompensates the OHT during the ceased freshwater hosing stage (Fig. 7c). In any cases, the BJC occurs very well at the decadal and longer time scales.

The main large-scale processes under freshwater perturbation are summarized in Fig. 8. It is plausible that the BJC can be well understood from the viewpoint of large-scale circulation changes. However, several questions remain. For instance, what are the intrinsic mechanisms determining different compensation structures in different latitudes? Why does the AHT undercompensate the OHT in the extratropical NH under freshwater forcing? How does the extratropical NH maintain its regional energy

balance, since it loses (gains) more energy through the OHT but gains (loses) less energy through the AHT during stage I (stage II)? These questions cannot be answered by only looking at the ocean–atmosphere circulation changes, even in a qualitative way. In our previous studies (Liu et al. 2016; Yang et al. 2016b), we proposed in a simple energy balance model that the BJC is intrinsically determined by the local climate feedback between surface temperature and the net radiation flux at the TOA. This mechanism will be investigated next using the coupled experiments.

## 4. Climate feedback and energy balance

### a. Principles

The occurrence of BJC results from the constraint of global energy conservation. This was first proposed by Bjerknes (1964). Mathematically, the Bjerknes hypothesis can be expressed simply as follows:

TABLE 1. BJC rate [ $C_R \equiv r(\sigma_{F_a}/\sigma_{F_o})$ ] in freshwater perturbation experiments.

FW01	$r\sigma_{F_a}/\sigma_{F_o}$			$r\sigma_{F_{\text{pac}}}/\sigma_{F_{\text{Atl}}} (30^{\circ}\text{S}$ – $30^{\circ}\text{N})$	$r\sigma_{F_a}/\sigma_{F_{\text{Atl}}} (30^{\circ}\text{S}$ – $30^{\circ}\text{N})$
	Global	Tropics ( $30^{\circ}\text{S}$ – $30^{\circ}\text{N}$ )	Extratropics ( $30^{\circ}\text{N}$ – $90^{\circ}\text{S}$ poleward)		
Stage I	$-0.97$	$-1.20$	$-0.54$	$-0.30$	$-0.86$
Stage II	$-1.11$	$-1.51$	$-0.61$	$-0.50$	$-0.90$

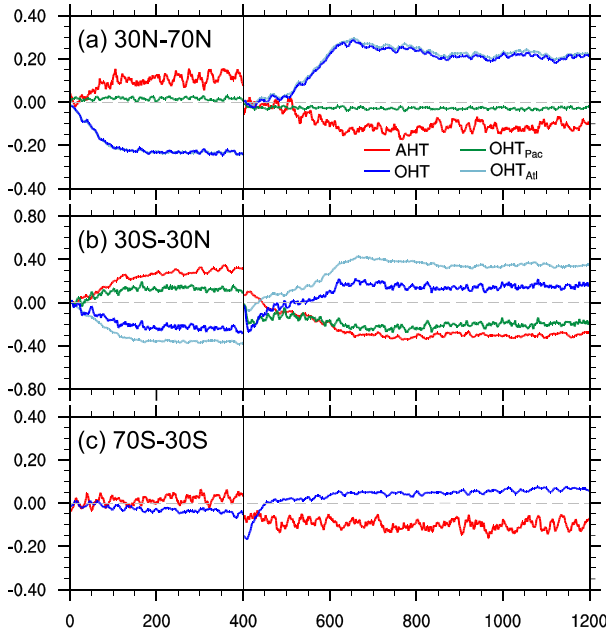


FIG. 7. Temporal evolutions of AHT (red), global total OHT (blue), Atlantic OHT (light blue), and Indo-Pacific OHT (green) in FW01 averaged in different latitude bands, for (a) 30°–70°N, (b) 30°S–30°N, and (c) 30°–70°S. Units: PW. During years 0–400, the heat transport changes are relative to the mean values of CTRL. During years 401–1200, the heat transport changes are relative to the mean values in stage I of FW01. All curves are smoothed with an 11-yr running mean.

$$\Delta F_a + \Delta F_o = 0 \Rightarrow \Delta F_a = -\Delta F_o, \quad (1)$$

where  $\Delta F_a$  and  $\Delta F_o$  are anomalous AHT and OHT, respectively. Without changes in energy flux at the TOA and ocean storage, the energy conservation for a given atmosphere–ocean box requires perfect compensation between inflowing AHT and outflowing OHT and vice versa. However, in a more general case, the TOA is not a rigid lid and there is always climate feedback between the energy flux at the TOA and surface temperature. We have proposed that the local climate feedback

determines the extent of BJC (Liu et al. 2016; Yang et al. 2016b). Then, Eq. (1) can be revised conceptually:

$$\Delta F_a + \Delta F_o = \Delta F_{\text{toa}}^B \Rightarrow \Delta F_a = \Delta F_{\text{toa}}^B - \Delta F_o, \quad (2)$$

where  $\Delta F_{\text{toa}}^B$  is net heat flux change at the TOA due to climate feedback  $B$ . The relative changes between AHT and OHT are actually determined by the climate feedback. Equation (2) still represents an energy conservation system, without considering the ocean heat storage change. Note that both the sign and the magnitude of climate feedback  $B$  are critical to the ratio  $\Delta F_a/\Delta F_o$ . Equation (2) implies big uncertainties to the BJC. For a very strong positive feedback ( $B \gg 0$ ),  $\Delta F_a$  and  $\Delta F_o$  can be the same sign and the BJC would fail (Yang et al. 2016b). On the other hand, for a very strong negative feedback ( $B \ll 0 \rightarrow |\Delta F_{\text{toa}}^B| \gg 0$ ) the BJC would also fail technically since the BJC rate  $\Delta F_a/\Delta F_o \rightarrow 0$  or  $\infty$ . This means any local energy imbalance can be damped locally in the vertical through the TOA. Of course,  $B = 0 \rightarrow \Delta F_{\text{toa}}^B = 0$ , and Eq. (2) is reduced to the Bjerknes hypothesis Eq. (1).

As in Dai et al. (2017), theoretically the BJC rate at the latitude boundary in a two-box system can be formulated as

$$C_R \equiv \frac{\Delta F_a}{\Delta F_o} = -\frac{1}{1 - B_1 B_2 [(B_1 + B_2)\chi]^{-1}}. \quad (3)$$

Equation (3) explicitly states that  $C_R$  is independent of the mean climate, changes in temperature and salinity, and the heat transports themselves. It is only determined by the local climate feedback parameters  $B_i$ , and the AHT coefficient  $\chi$ . In a stable climate system,  $B_i < 0$  usually, representing an overall negative climate feedback; therefore,  $C_R$  is always negative ( $C_R < 0$ ), or the changes in AHT and OHT always compensate each other. Since  $\chi$  is always positive and less uncertain (North 1975; Marotzke and Stone 1995), we will focus on  $B_i$  in this paper.

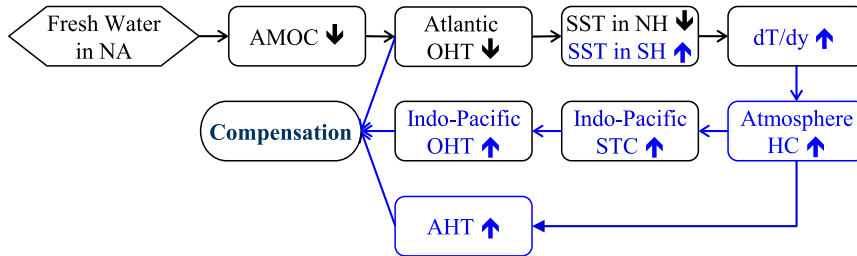


FIG. 8. Schematic diagram showing the main processes that are responsible for the compensation change between AHT and OHT. The upward (downward) arrows represent increase (decrease). NA: the North Atlantic; AMOC: the Atlantic MOC; STC: the subtropical cell; HC: the Hadley cell; OHT (AHT): the ocean (atmosphere) heat transport.  $dT/dy$  represents the northward SST gradient.



The BJC depicted in Eqs. (1)–(3) is illustrated in Fig. 9, which shows conceptually how the energy balance at the TOA and the climate feedback determine the BJC at the box boundary (Latitude-1 in Fig. 9) in a two-box system. If one local climate feedback is zero ( $B_1$  or  $B_2 = 0$ ), the AHT will perfectly compensate the OHT ( $\Delta F_a = -\Delta F_o$ ,  $C_R = -1$ ). This is the situation of Eq. (1). If the local negative climate feedback is extremely strong, any local heat imbalance will be effectively damped locally and the BJC will fail technically ( $B_1$  or  $B_2 \rightarrow \infty$ ,  $C_R \rightarrow 0$ ). In common cases, the climate feedbacks are not zero ( $B_1, B_2 \neq 0$ ) and the relative magnitudes of  $\Delta F_a$  and  $\Delta F_o$  at the box boundary in a two-box system are determined by the net heat flux at the TOA ( $\Delta F_{toa}^B$ ), which, in turn, is determined by the climate feedback in the two boxes (Fig. 9). So, the climate feedback plays a critical role in the energy balance for a regional box. It can be positive or negative (in a reasonable range), resulting in overcompensation ( $|C_R| > 1$ ) or undercompensation ( $|C_R| < 1$ ). Equation (3) provides a theoretical explanation for different BJC behaviors in various modeling studies (e.g., Kang et al. 2008, 2009; Vellinga and Wu 2008; Enderton and Marshall 2009; Vallis and Farneti 2009; Zhang et al. 2010; Farneti and Vallis 2013; Yang et al. 2013; Seo et al. 2014).

In a more common situation when the ocean heat storage change is considered, however, the energy balance in a local air–sea box is expressed by

$$\Delta F_a + \Delta F_o = \Delta F_{toa}^B + \Delta H_S \Rightarrow \Delta F_a = \Delta F_{toa}^B + \Delta H_S - \Delta F_o, \quad (4)$$

where  $\Delta F_S$  is the local ocean heat storage change. Equation (4) states that there could be no OHT change (i.e., no BJC) if local ocean energy gain (loss) through the surface is completely used to change the ocean heat storage. This would occur in climate variability at short time scales or in a transient stage of climate change. However, Fig. 7 shows that the BJC is also valid in the transient stage of freshwater forcing. Even during the quasi-equilibrium state, the heat storage change is not zero (Fig. 4) but the BJC is well established (Fig. 6). Therefore, it will be very interesting to see how the BJC predicted by Eq. (3) is modified quantitatively in the presence of ocean heat storage change.

### b. Climate feedbacks at different latitudes

At most latitudes, there are good linear relationships between changes in radiation flux at the TOA and surface temperature. This suggests a very stable climate feedback during both the transient and equilibrium stages of freshwater forcing. Figure 10 is the scatterplot for the radiation flux change versus the SAT change for the whole 1200 years. Simple linear regression is used to determine

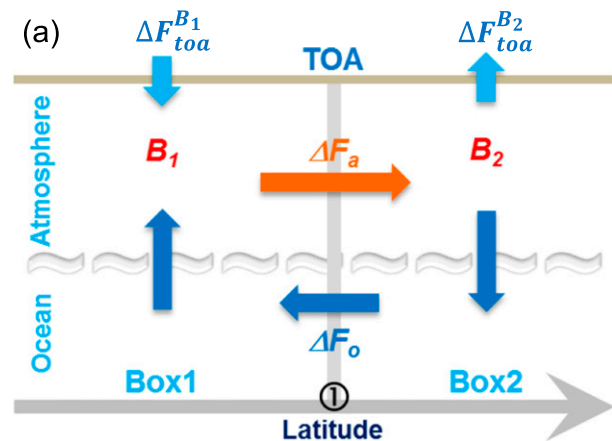


FIG. 9. Schematic diagram showing the BJC mechanism. The energy is conserved for each atmosphere and ocean box. The horizontal arrows represent the anomalous heat transports across the latitude boundary of ocean–atmosphere box, and the vertical arrows represent the anomalous heat fluxes at the ocean surface and the TOA.  $\Delta F_a$  and  $\Delta F_o$  represent anomalous AHT and OHT, respectively.  $B_1$  and  $B_2$  represent climate feedbacks in regional boxes. In a two-box situation, the BJC at latitude-1 is determined by the climate feedbacks  $B_1$  and  $B_2$  as formulated in Eq. (3). [Reproduced from Fig. 7a of Dai et al. (2017)].

the feedbacks related to the net SW, LW, and cloud radiative forcing (CRF) at the TOA. A similar approach was used in Rose and Marshall (2009). The CRF is calculated from the all-sky SW (LW) minus the clear-sky SW (LW), representing the integrated cloud effect on SW (LW). The regression coefficient represents the climate feedback, shown as the slope of each straight line in Fig. 10. Readers who are interested in the patterns of net SW, LW, and CRF changes, as well as the changes of low and high clouds, can refer to the appendix.

In the extratropical NH, there is an overall negative feedback between the net heat flux and SAT (Fig. 10a). This negative feedback is mainly due to the strong negative feedback related to the LW and surface temperature (Fig. 10d), which overcomes the strong positive feedback related to the SW (Fig. 10b). The strong cooling (warming) in the extratropical NH in stage I (stage II) results in significant reductions (increases) in both the outgoing LW and net incoming SW (Figs. A1 and A2 in the appendix). The feedbacks related to the SW CRF (Fig. 10c) and LW CRF (Fig. 10e) show opposite signs to the total SW and LW feedback, suggesting that other processes (such like sea ice) dominate the total SW and LW feedback there (see detailed discussions in the appendix).

In the tropical NH, there is an overall positive feedback between the net heat flux and SAT (Fig. 10f). This positive feedback is also due to the strong positive LW feedback (Fig. 10i), which in turn results from the LW CRF (Fig. 10j). The clouds play an important role in changing

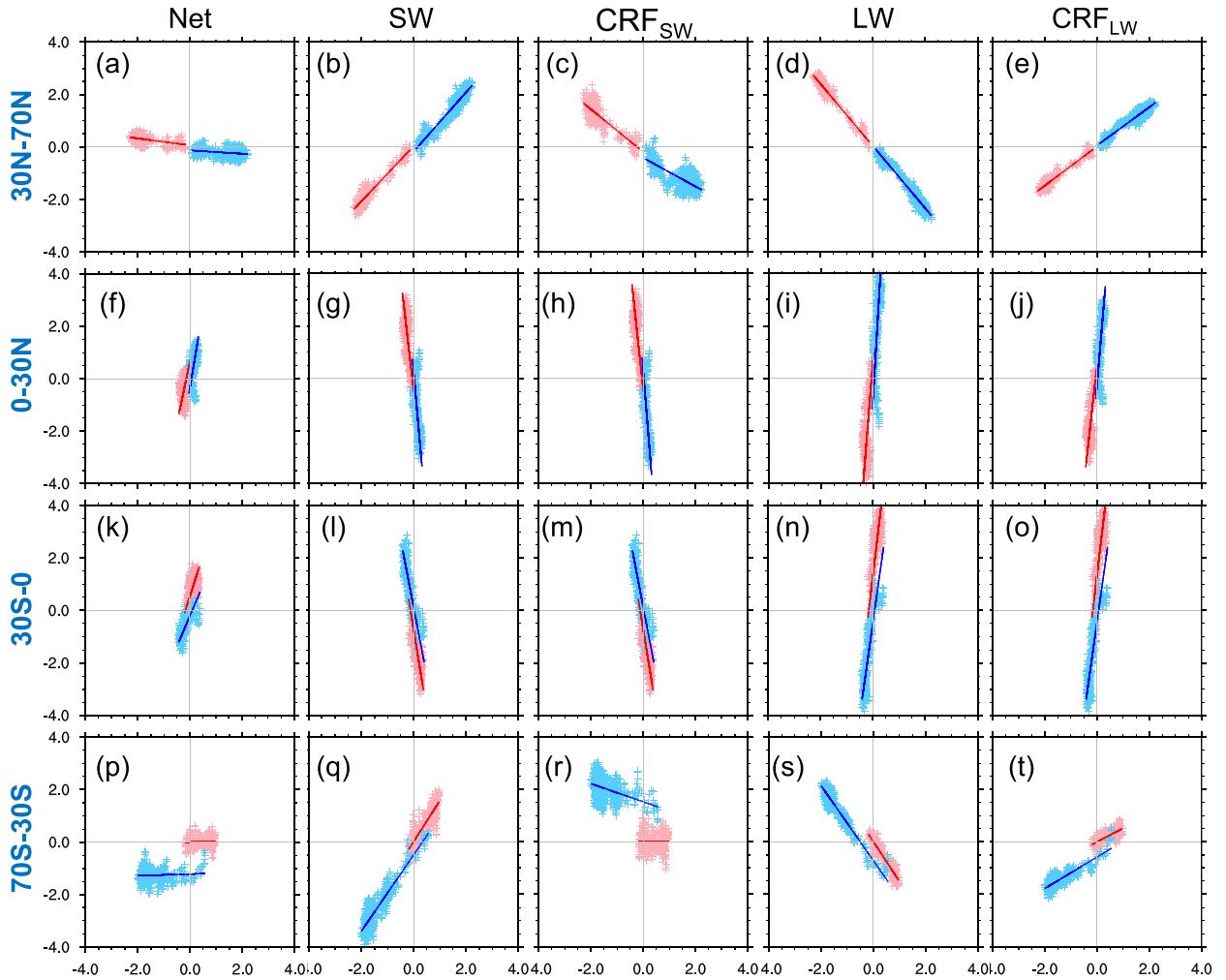


FIG. 10. Scatterplots for radiation flux change ( $y$  axis) vs SAT change ( $x$  axis). Red plus signs indicate for individual years during years 1–400, including the transient period and equilibrium stage (stage I) under freshwater hosing; blue pluses, for individual years during years 401–1200, including transient period and stage II after freshwater hosing ceased. The solid lines are linear regression lines of the scatter dots, in which positive (negative) slope represents positive (negative) climate feedback (units:  $\text{W m}^{-2} \text{K}^{-1}$ ). From the upper to lower panels, the values are averaged over  $30^{\circ}$ – $70^{\circ}\text{N}$ ,  $0^{\circ}$ – $30^{\circ}\text{N}$ ,  $30^{\circ}\text{S}$ – $0^{\circ}$ , and  $70^{\circ}$ – $30^{\circ}\text{S}$ , respectively.

the net radiative flux in the tropics. Both the SW CRF and LW CRF show similar patterns with the total SW and LW forcing (Figs. A1e,f). The total SW and LW feedbacks are entirely determined by the CRF feedbacks (Figs. 10g,h and Figs. 10i,j, respectively). The negative SW CRF feedback is mainly due to the change in the low clouds (Fig. A1h). The cooling in the NH reduces the convection in the deep tropics, resulting in less low clouds and less SW reflected back to the space. The positive LW CRF feedback is associated with the high cloud change (Fig. A1i). The NH cooling (SH warming) decreases (increases) the deep convection in the NH (SH) deep tropics, resulting in a significant reduction (increase) in high clouds, which in turn enhances (reduces) the outgoing LW and leads to TOA

radiation changes. These processes have been investigated in detail in Zhang et al. (2010).

In the tropical and extratropical SH, the feedback situations are roughly symmetric to those in the NH (Figs. 10k–t). One exception occurs in SW CRF in the extratropical SH (Fig. 10r), which does not affect the net SW feedback. In summary, we see that climate feedbacks at most latitudes are very stable in response to freshwater perturbation, regardless of the freshwater hosing period (red lines in Fig. 10) or recovering period (blue lines in Fig. 10), or of the transient stage or the equilibrium stage. The climate feedback parameters diagnosed in Fig. 10 can be brought into Eq. (3), to calculate the BJC theoretically in a complex Earth system. By comparing with the BJC rate obtained directly from model output of MHT, one can better

understand the fundamental mechanisms of the BJC in a complex system, assess the validity of theoretical BJC, and further estimate to what extent the BJC can be affected by ocean energy imbalance as shown in Eq. (4).

### c. Energy balance and BJC in FW01

Now, let us use the two-box conceptual model (Fig. 9) and Eq. (3) to understand the roles of local energy conservation and climate feedback in the BJC in FW01. To better discuss the regional energy balance and climate feedback, regional boundaries need to be set first. To be consistent, 30°N/S and the equator are again selected to focus on the tropics and extratropics, as well as the interhemispheric contrast. As we have done in Dai et al. (2017), here we want to emphasize that the boundary selection is *arbitrary*, which can be along *any* latitude. For any given regional box, energy should be balanced in an equilibrium state. For an atmosphere box, its energy budget consists of heat fluxes from the (ocean and land) surface and the TOA, as well as the meridional AHT across the selected latitudes. For an ocean box, its energy budget consists of heat fluxes across the ocean surface, the meridional OHT across the selected latitudes, and the ocean heat storage change.

Energy budget terms in FW01 are illustrated in Figs. 11 and 12. All values have an error bar of  $\pm 0.02$  PW, which is estimated as one standard deviation of MHT based on Figs. 6b and 6d. First of all, there is an energy surplus of about 0.10 PW manifested at the TOA (Fig. 11a) and the ocean surface (Fig. 11c) in stage I. This energy gain results from less outgoing LW and less latent heat loss from the ocean surface in response to the surface cooling in the NH. It is used to increase the ocean storage in the subsurface as shown in Fig. 4. We estimate that this 0.10-PW energy imbalance corresponds to about  $0.2 \text{ W m}^{-2}$  radiative flux imbalance at the TOA, which is in fact insignificant to the global energy balance. The terms  $\Delta F_a$  and  $\Delta F_o$  across the equator and 30°N are plotted in Figs. 11 and 12 as thick red and blue arrows, respectively. The net MHT change,  $\Delta F_t = |\Delta F_a| - |\Delta F_o|$ , shows an overcompensation in the tropics and SH and undercompensation in the extratropical NH (Fig. 11b).

The overcompensation in the tropics in stage I, which is particularly clear at the equator, is due to the strong overall positive feedback in the SH (black bar in the left cluster, Fig. 11d). This is consistent with the prediction by Eq. (3). The AHT overcompensates the OHT by about 40% at the equator. In the SH, the weak surface warming (Fig. 11d) is further enhanced by the net downward radiation flux (Fig. 11a). That is, a strong positive feedback occurs there. In the NH, the overall radiation flux change is neutral, and so is the overall

feedback (black bar in the right cluster), regardless of the strong surface cooling. In response to the weakened AMOC, the NH ocean gains about 0.34 PW through the surface by reducing surface LW and latent heat loss (Fig. 11d), in which about 0.09 PW energy is used to increase ocean heat storage, and the remaining 0.25 PW is transported to the SH across the equator. The NH atmosphere loses 0.34 PW of energy to the ocean and it is hardly made up by the energy gain at the TOA; therefore, strong AHT across the equator is needed to maintain the NH energy balance, resulting in overcompensation. This overcompensation can also be understood based on the energy balance in the SH. The SH ocean gains and exports 0.23 PW to the atmosphere. Because of the positive feedback in the SH, the SH atmosphere gains another 0.12 PW from the TOA. These two energy gains have to be exported to the NH to maintain the SH energy balance, resulting in overcompensation at the equator.

The energy balance situations in the two hemispheres in stage II are similar to those in stage I, but with opposite signs (Figs. 11e–h). Note that the 0.1-PW ocean energy gain in the NH in stage I is completely released to the atmosphere in stage II (Figs. 11g and h). Similar strong overcompensation occurs in the tropics, due to the strong positive feedback in the SH (black bar in the left cluster, Fig. 11h). The global overall feedback is also shown in Figs. 11d and 11h (bars in the middle cluster). In stage I (Fig. 11d), the global overall feedback is negative. The global-mean SAT change is about  $-0.30^\circ\text{C}$ , while there is a net energy gain of about 0.10 PW at the TOA. This negative feedback is mainly attributed to the negative LW change (red bar in the middle cluster). On global average, the SW CRF (cyan bar in the middle cluster) plays a role similar to that of LW. In stage II (Fig. 11h), however, the global overall climate feedback is strongly positive, because the global-mean SAT change in this stage is negative and very small ( $-0.11^\circ\text{C}$ ), and the net energy loss at the TOA is big ( $-0.10$  PW). The latter is due to the energy release of ocean storage in stage I, in association with the climate recovery after the freshwater hosing stops. The small global surface cooling occurs because the NH warming is counteracted by the strong surface cooling in the Southern Ocean. The latter is in turn caused by the strong positive sea ice–albedo feedback.

The undercompensation in the extratropical NH can be similarly understood based on the two-box approach (Fig. 12). In stage I, the AHT undercompensates the OHT by about 20% at 30°N (Figs. 12b,d), which is due to the overall negative feedback in this region (black bar in the right cluster), because the strong surface cooling results in less outgoing LW at the TOA (Fig. 12a). Note that  $\Delta F_o$  across 30°N is about 0.32 PW equatorward (Fig. 12d), in response to the weakened AMOC. The ocean gains about

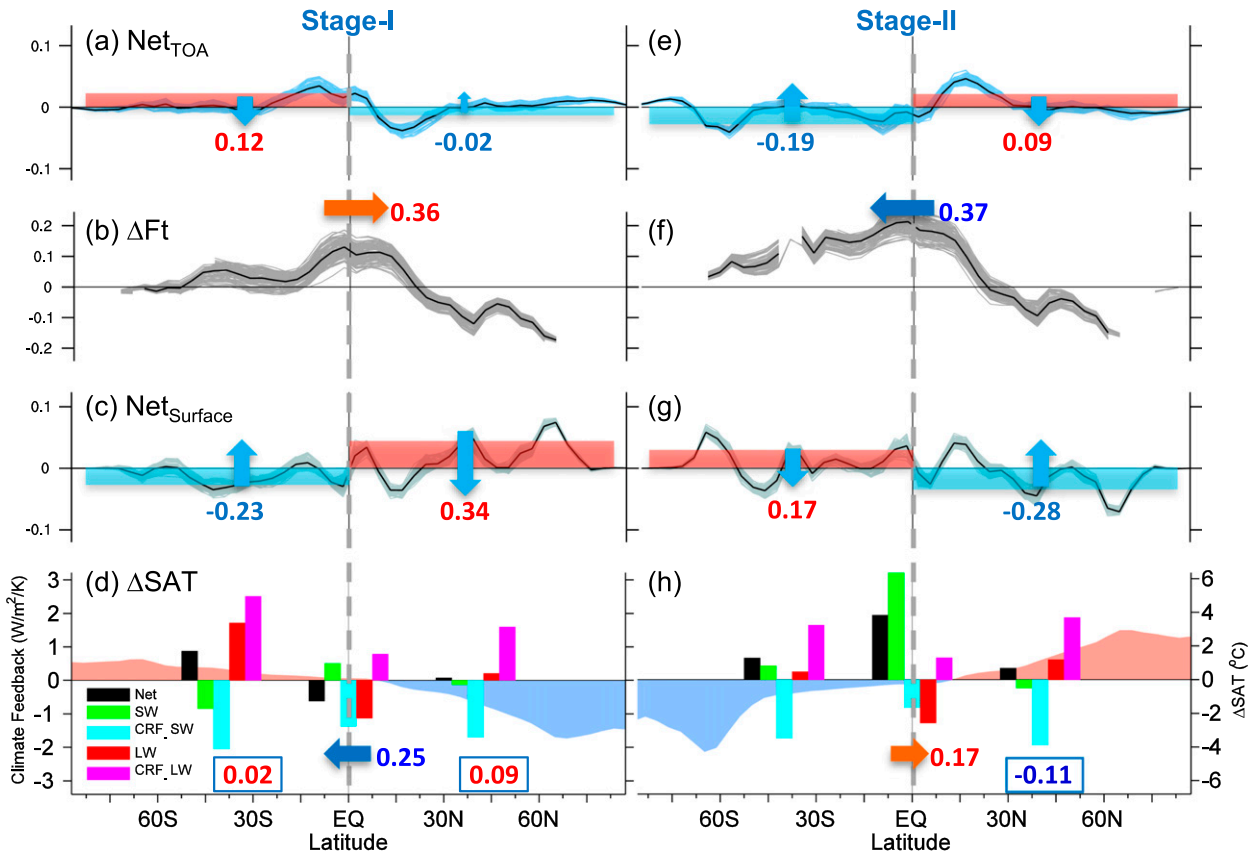


FIG. 11. Interhemispheric energy budget and BJC at the equator in FW01. (a) The net flux change at the TOA. (b) The net MHT change  $\Delta F_t$ , which is plotted only when  $\Delta F_a$  and  $\Delta F_o$  have different signs. (c) The net heat flux change at the ocean surface. (d) Zonally averaged  $\Delta\text{SAT}$  ( $^{\circ}\text{C}$ , shade curve). In (a) and (c), the fluxes ( $\text{W m}^{-2}$ ) have been converted to PW by multiplying the areas for easy comparison with MHT, and the values show area-integrated outgoing (blue) and incoming (red) energy over the SH and NH, respectively. In (b) and (d), the arrows and values show the direction and magnitude of  $\Delta F_a$  and  $\Delta F_o$  across the equator, respectively. In (a)–(c), the solid thick black curves represent 200-yr-mean values; the light gray curves are for individual years, but smoothed with the 11-yr running mean. The light gray curves show qualitatively the spread of each variable at decadal and longer time scales. Note that all the values have an error bar of  $\pm 0.02$  PW. The color bars in (d) show climate feedback ( $\text{W m}^{-2} \text{K}^{-1}$ ) in the SH (left cluster), the NH (right cluster) and globally (middle cluster), which are obtained by dividing the regional area-weighted heat flux by area-weighted  $\Delta\text{SAT}$ . Different color bars represent climate feedbacks by different processes. The positive (negative) value represents positive (negative) climate feedback. The positive (negative blue) number in the box shows the ocean heat storage increase (decrease) in that ocean box.

0.36 PW through the surface by reducing surface LW and latent heat loss (Fig. 12d). There is about a 0.04-PW ocean heat storage increase due to the interior ocean warming. The reduced outgoing LW at the TOA can partially offset the atmosphere heat loss (to the ocean). The remaining energy needed to maintain the atmosphere energy balance comes from the northward  $\Delta F_a$ . We see that  $\Delta F_a$  undercompensates  $\Delta F_o$  because the atmosphere does not need exactly 0.36 PW of energy from low latitudes, and part of its energy loss can be made up by the energy gain at the TOA (0.08 PW), which is in turn determined by the negative feedback in the extratropical NH (Fig. 12d). In stage II, the AHT undercompensates the OHT by about 10% (Figs. 12f,h). The energy balance situations are similar to those in stage I, and we will not discuss them further.

Similar analysis on the overcompensation in the extratropical SH can be made easily following the same approach, and we will not repeat the discussion (not shown). In general, energy is balanced for every latitude box within the error bar ( $\pm 0.02$  PW), when taking into account of ocean heat storage change. Also, how the AHT compensates the OHT depends on the climate feedback. In particular, the sign of climate feedback is critical to the behaviors of BJC. The regional feedbacks are obtained based on Figs. A1 and A2. The undercompensation across  $30^{\circ}\text{N}$  is due to the overall negative feedback in the extratropical NH (black bar in the right cluster, Figs. 12d,h). As discussed in the appendix, the strong negative LW feedback (red bar in the right cluster) dominates over the strong positive

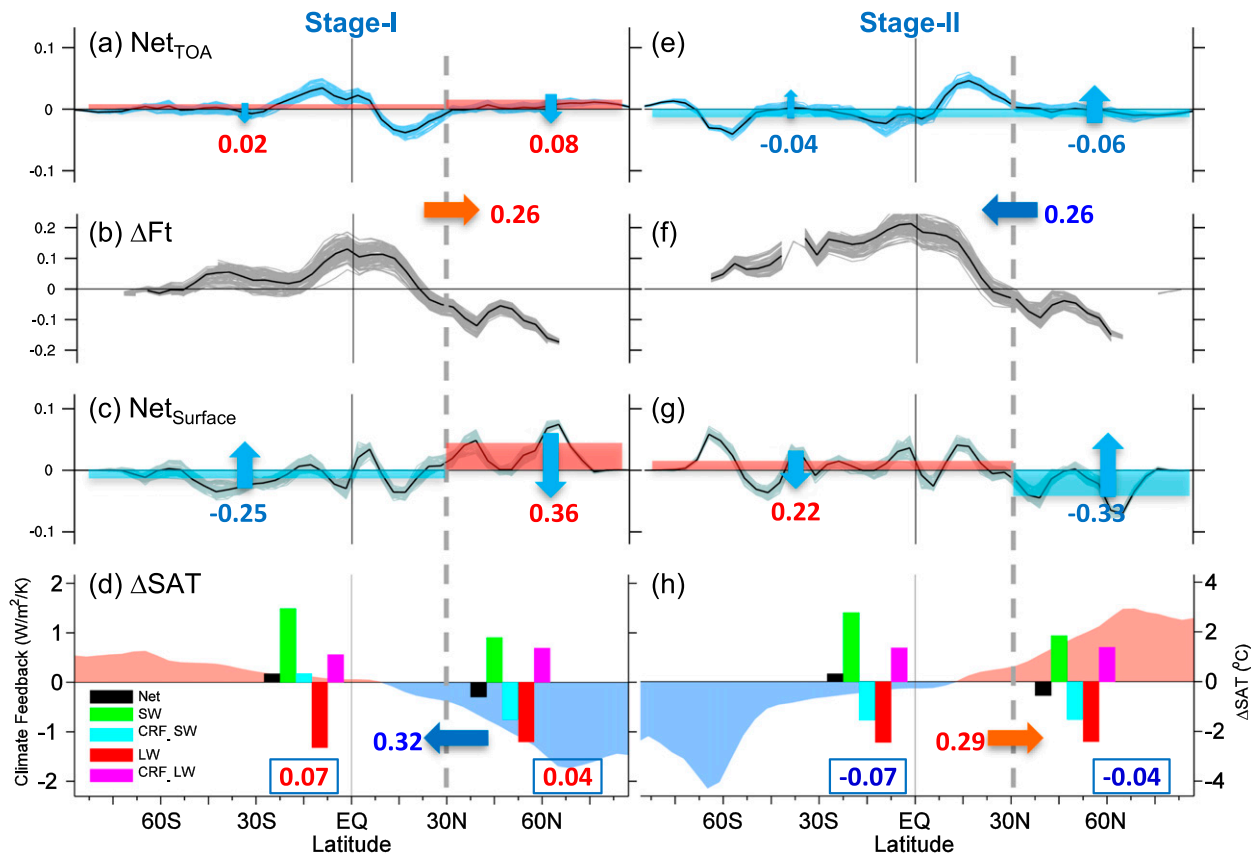


FIG. 12. As in Fig. 11, but for BJC across 30°N. In (a) and (c), the values show area-integrated outgoing (blue) and incoming (red) energy over 90°–30°S and 30°–90°N, respectively. In (b) and (d), the arrows and values show the direction and magnitude of  $\Delta F_a$  and  $\Delta F_o$  across 30°N, respectively. The color bars in (d) show climate feedbacks averaged within 90°–30°N (left cluster) and 30°–90°N (right cluster).

SW feedback (green bar), resulting in an overall negative feedback of about  $-0.30 \text{ W m}^{-2} \text{ K}^{-1}$  (black bar). The feedbacks related to LW CRF (magenta red bar) and SW CRF (cyan bar) are positive and negative, respectively, and they tend to offset the total LW and SW effect.

Based on the climate feedbacks shown in Figs. 11 and 12, the theoretical  $C_{R\text{theory}}$  can be estimated using Eq. (3) (Table 2). The model  $C_{R\text{model}} (= \Delta F_a / \Delta F_o)$  across 30°N/S and the equator can also be easily obtained based on model output. Although it is based on a highly simplified box model by Yang et al. (2016b),  $C_{R\text{theory}}$  is mostly consistent with  $C_{R\text{model}}$ , implying that the intrinsic mechanism of BJC is captured by the theory, which in turn sheds light on the BJC in a more complex system. However, the inconsistency between theory and model is also obvious. For example,  $C_{R\text{model}}$  across 30°S shows overcompensation in both stages I and II, whereas  $C_{R\text{theory}}$  shows a weak undercompensation. On the other hand,  $C_{R\text{model}}$  across 30°N shows a weak undercompensation in both stages I and II, while  $C_{R\text{theory}}$  shows a strong overcompensation, due to the overall positive feedback in the region south of 30°N. These

inconsistencies are actually expected because of ocean heat storage change based on Eq. (4). We have verified in another set of coupled model experiments that  $C_{R\text{model}}$  and  $C_{R\text{theory}}$  are qualitatively consistent at any latitudes (Dai et al. 2017). In an equilibrium state without ocean heat storage change,  $C_{R\text{model}}$  should also be intrinsically determined by the climate feedback, although the extent of overcompensation (undercompensation) suggested by  $C_{R\text{model}}$  and  $C_{R\text{theory}}$  can be slightly different.

## 5. Summary and discussion

The fundamental mechanism of BJC in a coupled Earth system is investigated in detail through freshwater perturbation experiments. This work focuses on the roles of energy balance and local climate feedback. Consistent with the theoretical studies of Liu et al. (2016) and Yang et al. (2016b), we confirm in this work that the energy constraint in a coupled system is a necessary condition for the occurrence of BJC, and the local climate feedback determines the extent of the BJC occurrence. Different



TABLE 2. Climate feedbacks related to different physical processes in three sensitivity experiments (units:  $\text{W m}^{-2} \text{K}^{-1}$ ) and the Bjerknes compensation rate ( $C_R$ ). For  $C_R$  on the equator,  $C_{R\text{model}} = \Delta F_a / \Delta F_o$  and it is calculated using the values on the equator in Fig. 12.  $C_{R\text{theory}}$  is obtained using Eq. (3), where  $B_1$  and  $B_2$  are the net mean climate feedbacks in the SH and NH, respectively (Yang et al. 2016b). For global overall  $C_R$ ,  $C_{R\text{model}}$  is the same as that in Table 1 and  $C_{R\text{theory}} = -[1/(1 - B/2\chi)]$ , where  $B$  is the global overall negative feedback. Here,  $\chi = 1.5 \text{ W m}^{-2} \text{K}^{-1}$ , based on previous studies (Marotzke and Stone 1995; Yang et al. 2015b). Note that  $\chi$  can be within a range of  $0.5 - 3.0 \text{ W m}^{-2} \text{K}^{-1}$  (North 1975), which would not change  $C_R$  qualitatively. Negative (positive) values represent negative (positive) feedback. The feedback value has an error of about  $\pm 0.01 \text{ W m}^{-2} \text{K}^{-1}$ .

	FW01	Global	SH	NH	90°–30°S	30°S–90°N	90°S–30°N	30°–90°N
Stage I	Net climate feedback	−0.63	0.89	0.08	−0.11	−0.41	0.18	−0.30
	$C_{R\text{model}}$	−0.97	−1.36		−1.07		−0.88	
	$C_{R\text{theory}}$	−0.83	−1.05		−0.95		−1.43	
Stage II	Net climate feedback	1.96	0.66	0.35	0.38	−0.09	0.16	−0.28
	$C_{R\text{model}}$	−1.11	−1.90		−2.0		−0.90	
	$C_{R\text{theory}}$	−2.88	−1.18		−0.85		−1.33	

compensation scenarios at different latitudes are due to different local climate feedbacks. Ocean heat storage change can affect the extent of BJC significantly, but will not change the BJC itself, even during the transient stage of climate change, as long as the total energy of the Earth system does not vary too much. Here we would also like to emphasize that the validity of BJC requires involvement of both atmosphere and ocean dynamics, and that meaningful BJC is only established at decadal and longer time scales (Zhao et al. 2016).

The compensation between the OHT in the Atlantic and that in the Indo-Pacific is clearly observed in the freshwater perturbation experiments. During the freshwater hosing stage, the weakened Atlantic OHT can be partially compensated by the enhanced Indo-Pacific OHT. The latter is caused by the enhanced HC in response to the enhanced meridional temperature gradient in the NH, which in turn is a result of weakened AMOC. It is the response in the Indo-Pacific that alleviates the global OHT change, and ultimately results in the overcompensation of the AHT to the OHT in the tropics. The concurrent changes between the HC and the Indo-Pacific OHT are consistent with the framework proposed in Held (2001), and can be well understood in the framework of wind-driven circulation, in which the ocean circulation is forced by the atmosphere. One more caveat is that although in principle we think the BJC works regardless of the location of the freshwater forcing applied, we are still very interested in the detailed responses in different freshwater situation, such as freshwater hosing in the North Pacific, along the equator, or in the Southern Oceans. We are working on this issue and hope to provide more insightful conclusions in the near future.

As we have emphasized in Dai et al. (2017), the BJC suggests an intrinsic connection between the radiative flux at the TOA and ocean circulations. In this work, we further show the critical role of the ocean thermohaline

circulation in regulating the global energy balance on decadal and longer time scales, by modulating local climate feedbacks. This work pays special attention to the roles of clouds. Low (high) clouds in different regions lead to different feedbacks (positive or negative), which can enhance or weaken the local surface response and thus local energy imbalance, modulating the BJC to some extent.

The conclusions in this work are generally consistent with previous studies (e.g., Vellinga and Wu 2008; Yang et al. 2013). However, the BJC mechanism proposed in this work is different from others. We want to emphasize that the BJC at certain latitude is determined by the climate feedbacks over the nearby regions, based on the two-box model illustrated in Fig. 9, instead of a heat budget at these latitudes (Vellinga and Wu 2008). In addition, previous studies showed that cloud feedback could make the tropical response much stronger, amplifying the impact on the shift of the tropical convection zone, weakening the compensation degree of the AHT and OHT (Kang et al. 2008; Zhang et al. 2010). However, in this work we notice that although the cloud feedback related to the LW and SW in the tropics is strong and dominates the total LW and SW feedbacks, the net cloud feedback is weak due to the cancelation of the positive LW cloud feedback and negative SW cloud feedback. It is still not obvious how the cloud feedback affects the BJC in the Earth climate system. This issue is being investigated in our ongoing research.

This work is a part of our series of studies on BJC in the Earth climate system (Yang and Dai 2015; Dai et al. 2017; Zhao et al. 2016). So far, we have examined the roles of energy conservation and local climate feedback in the BJC in the wind perturbation experiments (Dai et al. 2017) and freshwater experiments. We are investigating the BJC under global warming in the Earth system model. Although our theoretical

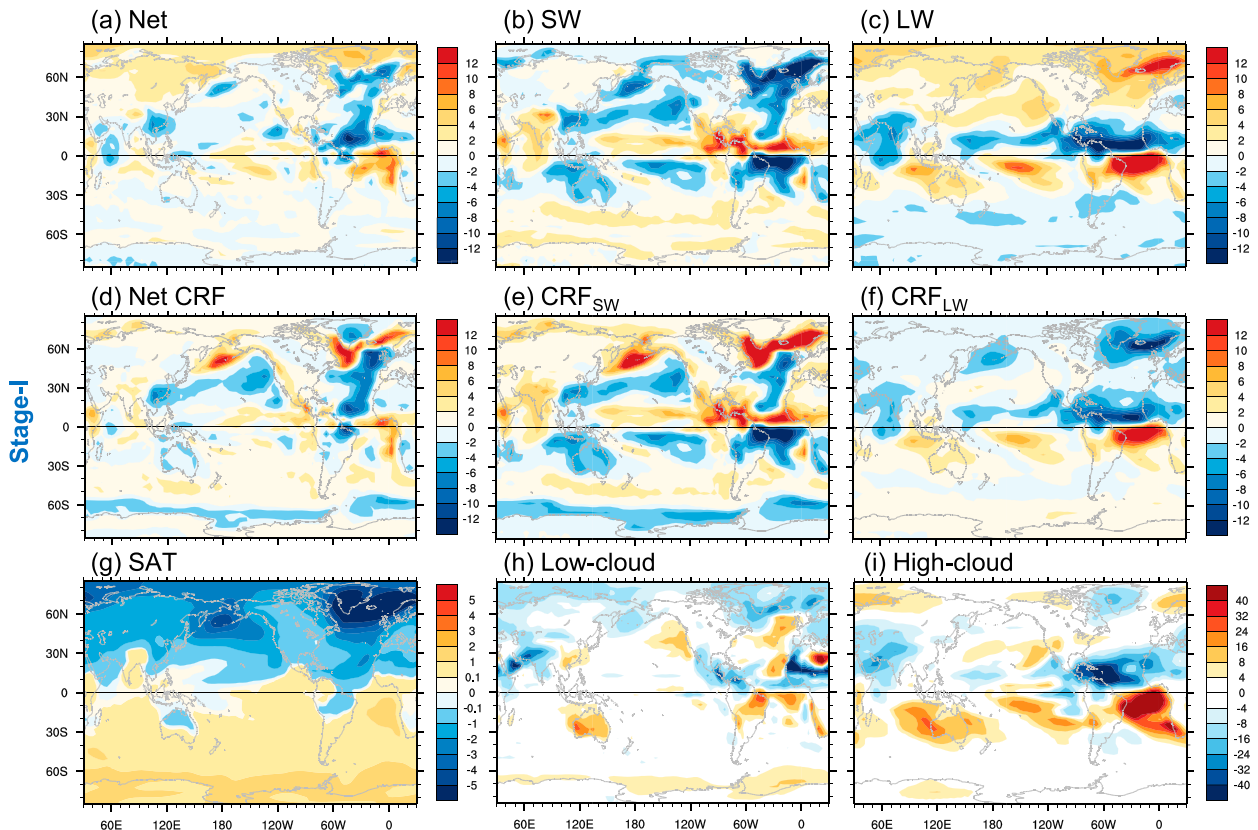


FIG. A1. Climate changes in stage I of FW01. (a) Net radiation flux change ( $\text{W m}^{-2}$ ), (b) net SW change, (c) net LW change at the TOA, (d) net cloud radiation forcing (CRF) ( $\text{W m}^{-2}$ ), (e) SW CRF, (f) LW CRF, (g) surface air temperature (SAT) change ( $^{\circ}\text{C}$ ), (h) low-cloud change, and (i) high-cloud change (unit: %). The CRF is calculated from the all-sky SW (LW) minus the clear-sky SW (LW). In the radiation flux plots, negative value represents radiation loss (outgoing) and positive value represents heat gain (incoming) at the TOA. The SAT cooling (warming) over the Northern (Southern) Hemisphere is about  $-1.14^{\circ}\text{C}$  ( $0.54^{\circ}\text{C}$ ).

study showed that the BJC will fail under greenhouse gas forcing because of the violation of global energy conservation (Yang et al. 2016b), it remains uncertain in a coupled complex model. Our preliminary results show that the BJC can be still valid to some extent under the global warming, if the freshwater perturbation caused by atmospheric heating dominates the change in ocean thermohaline circulation. Under the present-day global warming rate, we still expect that the BJC plays a stabilizing role in containing Earth's climate shift. How would the climate feedbacks in a warming climate adjust to assure the occurrence of BJC? Is there a threshold of global warming rate beyond which the BJC would completely fail? We are seeking answers to these questions.

*Acknowledgments.* This work is jointly supported by the NSF of China (Grants 41376007, 41176002, and 91337106). All experiments were performed on the supercomputer at the LaCOAS of Peking University.

## APPENDIX

### Radiation Flux at the Top of Atmosphere, Clouds, and Cloud Radiative Forcing

To better understand the BJC in the freshwater perturbation experiments reported in this study, the radiation flux balance at the TOA is examined here. Figure A1 shows components of net heat flux changes at the TOA in stage I of FW01. The CRF deserves special attention here, which is calculated from the all-sky SW (LW) minus the clear-sky SW (LW), representing the integrated cloud effect on SW and LW. To help understand CRF, anomalous low-cloud ( $p > 680$  hPa) and anomalous high-cloud ( $p < 440$  hPa) variables (as defined in Zhang et al. 2010) are also plotted.

The net TOA radiation flux change shows an energy loss (gain) over the ocean (land and sea ice) in the NH (Fig. A1a). This suggests an overall positive (negative)

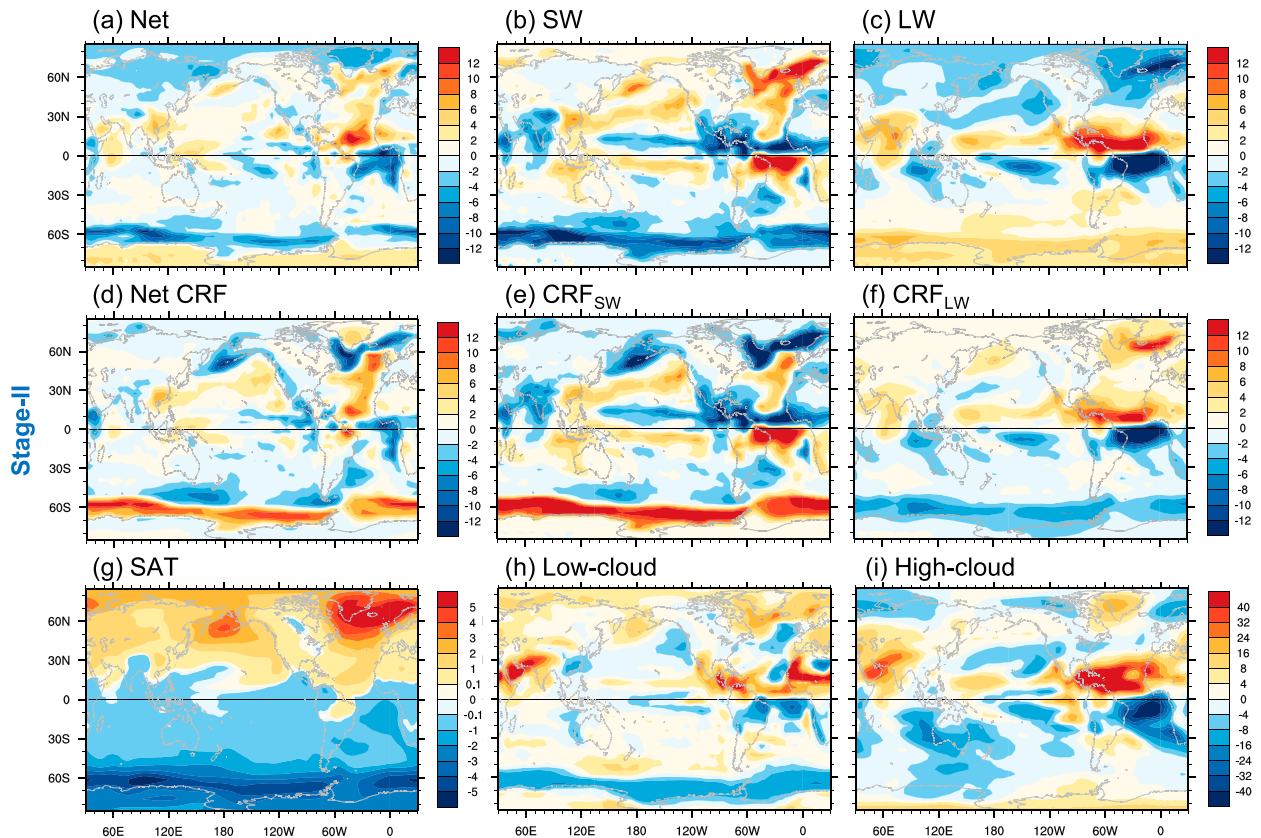


FIG. A2. As in Fig. A1, but for stage II of FW01. The SAT warming (cooling) over the Northern (Southern) Hemisphere is about  $0.93^{\circ}\text{C}$  ( $-1.15^{\circ}\text{C}$ ).

climate feedback over the ocean (land and sea ice), given the strong cooling in the NH (about  $-1.14^{\circ}\text{C}$ ) (Fig. A1g). The TOA energy loss over the ocean is mainly due to the reduction in the net incoming SW in the extratropics (Fig. A1b) and the increase in the outgoing LW in the tropics (Fig. A1c). The positive radiation flux change in the NH polar latitudes is due to positive LW change, suggesting a negative climate feedback over the region. The ocean energy loss occurs mainly in the North Atlantic, in association with strong cooling in SST. The net TOA radiation flux change over the SH shows a weak uniform energy loss (gain) in the extratropics (tropics), suggesting an overall negative (positive) climate feedback in the extratropics (tropics). This pattern is dominated by the LW change in the SH.

Cloud plays an important role in net radiative flux in the middle to low latitudes (between  $50^{\circ}\text{S}$  and  $50^{\circ}\text{N}$ ). In this region, both SW CF and LW CRF show similar patterns as the total SW and LW forcing (Figs. A1e,f). Specifically, over the midlatitude ocean the negative SW CRF (Fig. A1e) dominates the SW change (Fig. A1b), and thus the net flux change (Fig. A1a).

This is particularly clear over the midlatitude Atlantic. This SW CRF change is mainly due to the increase in low cloud coverage (Fig. A1h). The cooling in the NH reduces the deep convection in the North Atlantic, resulting in more stratus clouds, which reflects more SW back to the space. The low clouds there play an important role in the positive feedback in SST change (i.e.,  $\text{SST}\downarrow \rightarrow \text{low cloud}\uparrow \rightarrow \text{SW}\downarrow \rightarrow \text{SST}\downarrow$ ). This process was investigated in detail in Zhang et al. (2010). Over the tropical ocean, the LW CRF (Fig. A1f) dominates the LW change (Fig. A1c), and thus the net flux change (Fig. A1a). This is associated with high-cloud change (Fig. A1i). The NH cooling (SH warming) decreases (increases) the deep convection in the NH (SH) deep tropics, resulting in a significant reduction (increase) in high cloud coverage, which in turn enhances (reduces) the outgoing LW and thus the TOA energy loss. Now, it is the high cloud coverage in the tropics that plays an important role in the positive feedback in SST change (i.e.,  $\text{SST}\downarrow \rightarrow \text{high cloud}\downarrow \rightarrow \text{outgoing LW}\uparrow \rightarrow \text{net LW}\downarrow \rightarrow \text{SST}\downarrow$ ).

In the high latitudes (poleward of  $50^{\circ}\text{N/S}$ ), the SW CRF and LW CRF show opposite signs from the total SW and LW forcing, suggesting that other processes

(such as sea ice) dominate the change in total SW and LW. For example, the decrease in low cloud coverage over the Bering Sea of the Pacific and over the Labrador Sea and Greenland–Iceland–Norwegian (GIN) Seas of the Atlantic (Fig. A1h) results in positive SW CRF (Fig. A1e), while the total SW change is negative (Fig. A1b), suggesting that the latter is due to enhanced sea ice reflection. The sea ice–albedo positive feedback relative to the SW dominates over the low-cloud negative feedback in terms of SW CRF. However, at the same time the decreases in both low cloud and high cloud over the same region result in more outgoing LW (Fig. A1f) since the temperature at the top of cloud is lower than the SST. This is a positive feedback between SST and clouds, in terms of LW CRF. The net LW change at the TOA is positive over the high latitudes (Fig. A1c), suggesting that the significant SST cooling directly causes strong reduction in the outgoing LW from the surface. This is a negative feedback, and overwhelms the positive cloud feedback (Fig. A1f) and stabilizes the SST change. In summary, in the high latitudes over the GIN Seas and Bering Sea, the sea ice–albedo–SST–SW positive feedback dominates over the SST–LW negative feedback, whereas over the Arctic, the Greenland and Euro-Asia continent the SST–LW negative feedback dominates.

A general positive feedback is observed over the ocean regardless of the mechanisms at work. This positive feedback is particularly clear in the North Atlantic, which plays a critical role in the rapid shutdown of the AMOC during freshwater hosing. It is also responsible for the rapid recovering and overshooting of the AMOC (Fig. 5a) once the freshwater hosing stops. Figure A2 shows the heat flux change at the TOA in stage II of FW01. We can see that all variables have opposite signs to those in stage I. Consistent with Fig. A1, similar conclusions can be obtained based on Fig. A2. Here, we want to emphasize that in both stages there is a negative feedback between the SAT and the TOA net radiation flux over the land and polar region, which should be stronger than the positive feedback over the ocean and ultimately stabilize the global climate.

#### REFERENCES

- Bjerknes, J., 1964: Atlantic air–sea interaction. *Advances in Geophysics*, Vol. 10, Academic Press, 1–82.
- Chang, P., and Coauthors, 2008: Oceanic link between abrupt changes in the North Atlantic Ocean and the African monsoon. *Nat. Geosci.*, **1**, 444–448, doi:10.1038/ngeo218.
- Cheng, W., C. M. Bitz, and J. C. H. Chiang, 2007: Adjustment of the global climate to an abrupt slowdown of the Atlantic meridional overturning circulation. *Ocean Circulation: Mechanisms and Impacts*, *Geophys. Monogr.*, Vol. 173, Amer. Geophys. Union, 295–313.
- Czaja, A., and J. Marshall, 2006: The partitioning of poleward heat transport between the atmosphere and ocean. *J. Atmos. Sci.*, **63**, 1498–1511, doi:10.1175/JAS3695.1.
- Dai, H., H. Yang, and J. Yin, 2017: Roles of energy conservation and climate feedback in Bjerknes compensation: A coupled modeling study. *Climate Dyn.*, doi:10.1007/s00382-016-3386-y, in press.
- Danabasoglu, G., S. Bates, B. P. Briegleb, S. R. Jayne, M. Jochum, W. G. Large, S. Peacock, and S. G. Yeager, 2012: The CCSM4 ocean component. *J. Climate*, **25**, 1361–1389, doi:10.1175/JCLI-D-11-00091.1.
- Enderton, D., and J. Marshall, 2009: Explorations of atmosphere–ocean–ice climates on an aquaplanet and their meridional energy transports. *J. Atmos. Sci.*, **66**, 1593–1611, doi:10.1175/2008JAS2680.1.
- Farneti, R., and G. Vallis, 2013: Meridional energy transport in the coupled atmosphere–ocean system: Compensation and partitioning. *J. Climate*, **26**, 7151–7166, doi:10.1175/JCLI-D-12-00133.1.
- Held, I. M., 2001: The partitioning of the poleward energy transport between the tropical ocean and atmosphere. *J. Atmos. Sci.*, **58**, 943–948, doi:10.1175/1520-0469(2001)058<0943:TPOTPE>2.0.CO;2.
- Hunke, E., and W. Lipscomb, 2010: CICE: The Los Alamos Sea Ice Model, documentation and software user’s manual, version 4.1. Los Alamos National Laboratory Tech. Rep. LA-CC-06-012, 74 pp.
- Kang, S. M., I. M. Held, D. M. W. Frierson, and M. Zhao, 2008: The response of the ITCZ to extratropical thermal forcing: Idealized slab-ocean experiments with a GCM. *J. Climate*, **21**, 3521–3532, doi:10.1175/2007JCLI2146.1.
- , D. M. W. Frierson, and I. M. Held, 2009: The tropical response to extratropical thermal forcing in an idealized GCM: The importance of radiative feedbacks and convective parameterization. *J. Atmos. Sci.*, **66**, 2812–2827, doi:10.1175/2009JAS2924.1.
- Langen, P. L., and V. A. Alexeev, 2007: Polar amplification as a preferred response in an idealized aquaplanet GCM. *Climate Dyn.*, **29**, 305–317, doi:10.1007/s00382-006-0221-x.
- Laurian, A., A. Lazar, and G. Reverdin, 2009: Generation mechanism of spiciness anomalies: An OGCM analysis in the North Atlantic subtropical gyre. *J. Phys. Oceanogr.*, **39**, 1003–1018, doi:10.1175/2008JPO3896.1.
- Lawrence, D. M., K. W. Oleson, M. G. Flanner, C. G. Fletcher, P. J. Lawrence, S. Levis, S. C. Swenson, and G. B. Bonan, 2012: The CCSM4 land simulation, 1850–2005: Assessment of surface climate and new capabilities. *J. Climate*, **25**, 2240–2260, doi:10.1175/JCLI-D-11-00103.1.
- Liu, Z., 1994: A simple model of the mass exchange between the subtropical and tropical ocean. *J. Phys. Oceanogr.*, **24**, 1153–1165, doi:10.1175/1520-0485(1994)024<1153:ASMOTM>2.0.CO;2.
- , H. Yang, C. He, and Y. Zhao, 2016: A theory for Bjerknes compensation: The role of climate feedback. *J. Climate*, **29**, 191–208, doi:10.1175/JCLI-D-15-0227.1.
- Manabe, S., and R. J. Stouffer, 1995: Simulation of abrupt climate change induced by freshwater input to the North Atlantic Ocean. *Nature*, **378**, 165–167, doi:10.1038/378165a0.
- Marotzke, J., and P. Stone, 1995: Atmospheric transports, the thermohaline circulation, and flux adjustments in a simple coupled model. *J. Phys. Oceanogr.*, **25**, 1350–1364, doi:10.1175/1520-0485(1995)025<1350:ATTCA>2.0.CO;2.



- Meehl, G. A., and Coauthors, 2013: Climate change projections in CESM1(CAM5) compared to CCSM4. *J. Climate*, **26**, 6287–6308, doi:10.1175/JCLI-D-12-00572.1.
- Neale, R. B., and Coauthors, 2010: Description of the NCAR Community Atmosphere Model (CAM5.0). NCAR Tech. Rep. NCAR/TN-486+STR, 268 pp. [Available online at [www.cesm.ucar.edu/models/cesm1.1/cam/docs/description/cam5\\_desc.pdf](http://www.cesm.ucar.edu/models/cesm1.1/cam/docs/description/cam5_desc.pdf).]
- , J. Richter, S. Park, P. Lauritzen, S. Vavrus, P. Rasch, and M. Zhang, 2013: The mean climate of the Community Atmosphere Model (CAM4) in forced SST and fully coupled experiments. *J. Climate*, **26**, 5150–5168, doi:10.1175/JCLI-D-12-00236.1.
- North, G. R., 1975: Theory of energy-balance climate models. *J. Atmos. Sci.*, **32**, 2033–2043, doi:10.1175/1520-0469(1975)032<2033:TOEBCM>2.0.CO;2.
- , 1984: The small ice cap instability in diffusive climate models. *J. Atmos. Sci.*, **41**, 3390–3395, doi:10.1175/1520-0469(1984)041<3390:TSICII>2.0.CO;2.
- Park, S., C. S. Bretherton, and P. J. Rasch, 2014: Integrating cloud processes in the Community Atmosphere Model, version 5. *J. Climate*, **27**, 6821–6856, doi:10.1175/JCLI-D-14-00087.1.
- Rose, B. E., and J. Marshall, 2009: Ocean heat transport, sea ice, and multiple climate states: Insights from energy balance models. *J. Atmos. Sci.*, **66**, 2828–2843, doi:10.1175/2009JAS3039.1.
- , and D. Ferreira, 2013: Ocean heat transport and water vapor greenhouse in a warm equable climate: A new look at the low gradient paradox. *J. Climate*, **26**, 2117–2136, doi:10.1175/JCLI-D-11-00547.1.
- Seo, J., S. M. Kang, and D. M. Frierson, 2014: Sensitivity of intertropical convergence zone movement to the latitudinal position of thermal forcing. *J. Climate*, **27**, 3035–3042, doi:10.1175/JCLI-D-13-00691.1.
- Shaffrey, L., and R. Sutton, 2006: Bjerknes compensation and the decadal variability of the energy transports in a coupled climate model. *J. Climate*, **19**, 1167–1181, doi:10.1175/JCLI3652.1.
- Smith, R. D., and Coauthors, 2010: The Parallel Ocean Program (POP) reference manual. Los Alamos National Laboratory Tech. Rep. LAUR-10-01853, 140 pp. [Available online at <http://www.cesm.ucar.edu/models/ccsm4.0/pop/>.]
- Stouffer, R. J., and Coauthors, 2006: Investigating the causes of the response of the thermohaline circulation to past and future climate changes. *J. Climate*, **19**, 1365–1387, doi:10.1175/JCLI3689.1.
- , D. Seidov, and B. J. Haupt, 2007: Climate response to external sources of freshwater: North Atlantic versus the Southern Ocean. *J. Climate*, **20**, 436–448, doi:10.1175/JCLI4015.1.
- Timmermann, A., and H. Goosse, 2004: Is the wind stress forcing essential for the meridional overturning circulation? *Geophys. Res. Lett.*, **31**, L04303, doi:10.1029/2003GL018777.
- Trenberth, K. E., and J. M. Caron, 2001: Estimates of meridional atmosphere and ocean heat transports. *J. Climate*, **14**, 3433–3443, doi:10.1175/1520-0442(2001)014<3433:EOMAAO>2.0.CO;2.
- Vallis, G. K., and R. Farneti, 2009: Meridional energy transport in the coupled atmosphere–ocean system: Scaling and numerical experiments. *Quart. J. Roy. Meteor. Soc.*, **135**, 1643–1660, doi:10.1002/qj.498.
- van der Swaluw, E., S. S. Drijfhout, and W. Hazeleger, 2007: Bjerknes compensation at high northern latitudes: The ocean forcing the atmosphere. *J. Climate*, **20**, 6023–6032, doi:10.1175/2007JCLI1562.1.
- Vellinga, M., and P. Wu, 2008: Relations between northward ocean and atmosphere energy transports in a coupled climate model. *J. Climate*, **21**, 561–575, doi:10.1175/2007JCLI1754.1.
- Wu, L., F. He, Z. Liu, and C. Li, 2007: Atmospheric teleconnections of tropical Atlantic variability: Interhemispheric, tropical–extratropical, and cross-basin interactions. *J. Climate*, **20**, 856–870, doi:10.1175/JCLI4019.1.
- Wunsch, C., 2005: The total meridional heat flux and its oceanic and atmospheric partition. *J. Climate*, **18**, 4374–4380, doi:10.1175/JCLI3539.1.
- Yang, H., and H. Dai, 2015: Effect of wind forcing on the meridional heat transport in a coupled climate model: Equilibrium response. *Climate Dyn.*, **45**, 1451–1470, doi:10.1007/s00382-014-2393-0.
- , Y. Wang, and Z. Liu, 2013: A modeling study of the Bjerknes compensation in the meridional heat transport in a freshening ocean. *Tellus*, **65A**, 18480, <http://dx.doi.org/10.3402/tellusa.v65i0.18480>.
- , Q. Li, K. Wang, Y. Sun, and D. Sun, 2015a: Decomposing the meridional heat transport in the climate system. *Climate Dyn.*, **44**, 2751–2768, doi:10.1007/s00382-014-2380-5.
- , Y. Zhao, Z. Liu, Q. Li, F. He, and Q. Zhang, 2015b: Heat transport compensation in atmosphere and ocean over the past 22,000 years. *Sci. Rep.*, **5**, 16661, doi:10.1038/srep16661.
- , K. Wang, H. Dai, Y. Wang, and Q. Li, 2016a: Wind effect on the Atlantic meridional overturning circulation via sea ice and vertical diffusion. *Climate Dyn.*, **46**, 3387–3403, doi:10.1007/s00382-015-2774-z.
- , Y. Zhao, and Z. Liu, 2016b: Understanding Bjerknes compensation in atmosphere and ocean heat transports using a coupled box model. *J. Climate*, **29**, 2145–2160, doi:10.1175/JCLI-D-15-0281.1.
- Zhang, R., and T. L. Delworth, 2005: Simulated tropical response to a substantial weakening of the Atlantic thermohaline circulation. *J. Climate*, **18**, 1853–1860, doi:10.1175/JCLI3460.1.
- , S. M. Kang, and I. M. Held, 2010: Sensitivity of climate change induced by weakening of the Atlantic meridional overturning circulation to cloud feedback. *J. Climate*, **23**, 378–389, doi:10.1175/2009JCLI3118.1.
- Zhao, Y., H. Yang, and Z. Liu, 2016: Assessing Bjerknes compensation for climate variability and its time-scale dependence. *J. Climate*, **29**, 5501–5512, doi:10.1175/JCLI-D-15-0883.1.